Acta Pharmaceutica Sinica B 2025;15(10):5366−5386

Chinese Pharmaceutical Association
Institute of Materia Medica, Chinese Academy of Medical Sciences

Acta Pharmaceutica Sinica B

www.elsevier.com/locate/apsb
www.sciencedirect.com

ORIGINAL ARTICLE

Anti-CD24 antibody-nitric oxide donor conjugates bearing a self-bioorthogonal cleavable linker

Jianbing Wu[a,†], Tianyue Cheng[b,†], Jiajun Xie[b,†], Ziyu Qian[a], Linhua Huang[b], Xun Yuan[a], Libang Zhang[a], Shan Yang[c], Yihua Zhang[a], Tonglin Xu[d,*], Juan Zhang[b,*], Zhangjian Huang[a,e,*]

[a]*State Key Laboratory of Natural Medicines, Center of Drug Discovery, China Pharmaceutical University, Nanjing 211198, China*
[b]*Antibody Engineering Laboratory, School of Life Science & Technology, China Pharmaceutical University, Nanjing 211198, China*
[c]*School of Pharmacy, Key Laboratory of Active Components of Xinjiang Natural Medicine and Drug Release Technology, Engineering Research Center of Xinjiang and Central Asian Medicine Resources, Xinjiang Medical University, Urumqi 830054, China*
[d]*Nantong Third People's Hospital, Affiliated Nantong Hospital 3 of Nantong University, Nantong 226006, China*
[e]*Xinjiang Key Laboratory of Neurological Disorder Research, the Second Affiliated Hospital of Xinjiang Medical University, Urumqi 830028, China*

Received 7 August 2024; received in revised form 19 February 2025; accepted 16 April 2025

KEY WORDS

Bioorthogonal chemistry;
Triple-negative breast cancer;
Antibody-nitric oxide donor conjugate;
Site-specific conjugation;
CD24;

Abstract Triple-negative breast cancer (TNBC) is a highly aggressive malignancy predominantly managed *via* chemotherapy. Our clinical sample analysis revealed a significant correlation between elevated CD24 expression in TNBC tumor cells and patient survival rates. We developed a novel antibody−drug conjugate (ADC), named **HN03**, consisting of an antibody with engineered cysteines for site-specific conjugation with a low toxic nitric oxide (NO) precursor as its payload through a novel Pt(IV)-mediated bioorthogonal self-cleavable linker. **HN03** specifically targets tumor cells expressing high levels of CD24, concurrently generating cisplatin and releasing NO upon activation. **HN03** also exhibited potent *in vitro* and *in vivo* antitumor activity. It significantly reduced tumor growth at various

*Corresponding authors.
E-mail addresses: f80a50@163.com (Tonglin Xu), zhangjuan@cpu.edu.cn (Juan Zhang), zhangjianhuang@cpu.edu.cn (Zhangjian Huang).
[†]These authors made equal contributions to this work.
Peer review under the responsibility of Chinese Pharmaceutical Association and Institute of Materia Medica, Chinese Academy of Medical Sciences.

https://doi.org/10.1016/j.apsb.2025.07.037

Tumor microenvironment;
Cisplatin;
Self-cleavable linker

doses, prevented tumor metastasis, with markedly lower toxicity than traditional chemotherapy agents. We found that a key mechanism of its action involved inducing apoptosis and endoplasmic reticulum stress, substantially decreasing the number of M2-type macrophages. Overall, HN03 stands out as a promising therapeutic option for TNBC, offering a targeted treatment with reduced side effects and the potential for improved outcomes. Furthermore, using Pt(IV) in the linker and an NO precursor as the payload enhances the versatility of the Antibody-NO donor Conjugate (ANC), offering new avenues for the design of the next generation of ADCs.

1. Introduction

Triple-negative breast cancer (TNBC) is a highly invasive subtype of breast cancer characterized by the absence of estrogen receptor, progesterone receptor, and human epidermal growth factor receptor 2 (HER2) expression[1]. TNBC is associated with a high recurrence rate, high metastasis rate, poor prognosis, and high mortality[2,3]. To date, chemotherapy remains the primary treatment for TNBC. Nevertheless, the good response of TNBC to chemotherapy agents cannot hide the associated toxic effects, and the disease frequently becomes resistant to these drugs following extended therapy[4]. Notably, individuals with TNBC exhibit an elevated response rate to platinum-based medications combined with other drugs, indicating that combination or synergistic approaches are promising strategies. Besides, effectively directing chemotherapy agents to specific tumor sites is imperative and necessitates immediate attention within the realm of drug investigation for this particular condition[5].

Antibody−drug conjugates (ADCs) represent a rising class of targeted therapeutics. They consist of a monoclonal antibody covalently attached to a small bioactive molecular payload *via* a linker[6,7]. In contrast with small-molecule drugs, ADCs exhibit precise targeting capabilities, and thereby have reduced off-target toxicity. Furthermore, ADCs demonstrate superior tumor-killing effects over simple antibody drugs. Consequently, ADCs have garnered significant attention from researchers in the field of antitumor drugs and are at the forefront of global innovative drug development[8]. Till March 2024, 15 ADCs have received approval for marketing globally; they include various antigens, such as CD33, CD30, CD22, CD79b, c-MET, HER2, Nectin-4, TROP2, BCMA, and TF. Additionally, more than 100 ADCs are at different stages of clinical development[9].

Classical ADC antitumor drugs consist of three essential components: 1) an antibody, 2) a linker ensuring the stability of ADCs in the circulatory system and regulating the release of small-molecule drugs upon reaching the target site (it can be categorized as "cleavable" and "noncleavable"), and 3) payloads, which exert a cytotoxic effect upon reaching the tumor site. Each component plays a crucial role on the stability, safety, and efficacy of the entire molecule[10-13].

Although significant advancements have been made in the development of ADCs, several challenges remain to be addressed. First, site-specific conjugation is crucial. As ADCs are biopharmaceuticals, their drug-like properties are intimately linked to the drug-to-antibody ratio (DAR)[14]. Site-specific conjugation strategies can substantially enhance the stability of the conjugate and improve the overall pharmacological properties of the entire ADC molecule[15]. Second, linkers with enhanced stability, improved selectivity, and innovative chemical structures need to be developed. These properties are vital for reducing the toxic side effects associated with ADCs[16]. Last but not least, there is room for improving the payload. Beyond the highly toxic drugs currently employed, the potential of using endogenous regulatory molecules to exert pharmacological effects warrants exploration[12,17].

Nitric oxide (NO) is a signaling molecule involved in numerous physiological and pathological processe[18,19]. In recent years, the role of high levels of NO in tumor biology has gained considerable interest, particularly its implications in the initiation, progression, and metastasis of tumors[20]. Research has indicated that elevated NO levels can trigger apoptosis in tumor cells, impede tumor cell proliferation, hinder tumor metastasis, and overcome multidrug resistance in tumors. Furthermore, NO enhances the efficacy of radiotherapy, chemotherapy, and immunotherapy[21]. Notably, the NO donor drug RRx-001 has exhibited antitumor effects by downregulating the CD47/SIRPα axis in the tumor immune system, while also demonstrating a favorable safety profile. These findings suggest that NO holds great potential for tumor therapy[22,23].

In view of the benefits of ADCs—including precise targeting, high selectivity, and well-established technology—we developed a new type of ADC, the antibody-nitric oxide conjugate (ANC). This first-generation ANC, combining a nitric oxide (NO) donor with a monoclonal antibody through a linker with a disulfide bond that responds to the redox environment of the tumor, demonstrated promising antitumor efficacy[24,25]. This innovative approach gained widespread attention and was featured in Hepatic Cell News (Volume 3.11 | Mar 29, 2019).

Upon further consideration, we concluded that the disulfide bond structure type of the linker used in the first-generation ADCs could be improved. Compared with tumor microenvironment-responsive activation, prodrug activation through the cleavage of a bond by bioorthogonal catalysis is one of the more advantageous methods currently available[26]. In our previous works, we discovered that Pt(II) could catalyze the cleavage of propynyl protecting groups, whereas Pt(IV) could not. Furthermore, Pt(IV) could be selectively reduced to Pt(II) at the tumor site[27]. Pt(IV) complexes exhibit enhanced kinetic inertness and stability compared to Pt(II) compounds like cisplatin, allowing them to remain intact during systemic circulation and minimize off-target effects. Interestingly, the unique reducing environment of tumor cells, characterized by elevated levels of reducing agents such as glutathione (GSH) and ascorbic acid (Vc), facilitates the selective reduction of Pt(IV) to its active Pt(II) form. This reduction occurs preferentially in tumor cells due to their higher reductive capacity, ensuring localized activation of the cytotoxic Pt(II) species[28].

Additionally, the generated Pt(II) can catalyze bioorthogonal reactions, such as the release of NO, further enhancing therapeutic efficacy through synergistic effects[29,30]. Thus, the tumor-specific reduction of Pt(IV) to Pt(II) is a key mechanism underlying the targeted action of Pt(IV) prodrugs.

Therefore, in this study, we integrated Pt(IV) into the linker design to develop a linker that can be activated through an integrated bioorthogonal self-catalyzed bond cleavage. Moreover, Pt (II) also possesses potential antitumor activity, and thereby can play a dual role. Additionally, our clinical analysis of TNBC samples revealed a high expression of CD24 at tumor sites, and this protein was closely associated with patient survival rates.

This paper reports the design of a novel generation of ADC drug that incorporates the aforementioned strategies. This approach entails the combination of an anti-CD24 monoclonal antibody for site-specific conjugation with a propynyl-protected NO precursor as the payload through a Pt(IV) chemotherapeutic prodrug as a linker. First, we closely analyzed clinical samples to confirm CD24 as an intervention target for TNBC. Next, we developed and synthesized the ANC **HN03**, and conducted detailed *in vitro* analysis of its bioorthogonal activation and activity. We also confirmed its ability to release NO and be internalized. Subsequently, we evaluated the effectiveness of **HN03** against TNBC using various animal models and investigated its apoptotic-inducing mechanism.

2. Results and discussion

2.1. CD24 expression in TNBC

CD24 is a highly glycosylated protein with a small protein core that is linked to the plasma membrane *via* a glycosylphosphatidylinositol anchor. CD24 is primarily expressed by immune cells but is often overexpressed in human tumors. In cancer, CD24 regulates cell migration, invasion and proliferation. Its expression is associated with poor prognosis and it is a cancer stemness marker[31].

To assess the viability of CD24 as a therapeutic target for TNBC, we performed a comparative analysis using data from the cancer genome atlas (TCGA) and genotype-tissue expression (GTEx) databases and the gene expression profiling interactive analysis online bioinformatics tool (http://gepia.cancer-pku.cn). The findings are presented in Fig. 1. Our primary objective was to compare the expression of CD24 in tumor tissues and normal tissues. We found that 18 of the 33 analyzed tumor types demonstrated increased CD24 expression. We observed this upregulation in various high-incidence cancers, including breast cancer, colorectal cancer, liver cancer, lung cancers (lung adenocarcinoma and lung squamous cell carcinoma), and ovarian cancer. Notably, breast cancer showed the most pronounced upregulation of CD24 (Fig. 1A and B). Additionally, in TNBC, CD24 expression was found to be significantly higher than that in normal breast cells as well as in ER^+/PR^+ (abbreviated as HR^+), or $HER2^+$ breast cancer tissues[32]. This finding underscores the potential of CD24 as a molecular target in TNBC treatment strategies.

Moreover, we investigated the relationship between CD24 expression levels and the overall survival period of patients. We found that patients with higher CD24 levels consistently experienced shorter overall survival periods than those with lower CD24 levels (Fig. 1C). This finding suggests that elevated CD24 expression serves as a prognostic indicator for patients with breast cancer.

To better represent the clinical scenario of patients, we collected and analyzed clinical samples, including 22 cases of TNBC, 19 cases of paracancer tissue, 10 cases of normal breast tissue, 3 cases of $HER2^+$ breast cancer, and 3 cases of HR^+ breast cancer. Fig. 1D and E, and Supporting Information Fig. S1 illustrate the immunohistochemistry (IHC) analysis results. Our analysis revealed that CD24 was relatively highly expressed across various breast cancer subtypes, particularly in TNBC, where more than 90% of the samples showed moderate to high positive expression. In contrast, normal tissues and paracancer tissues exhibited relatively low CD24 expression. These findings align with the those of the database analysis and corroborate the observations of other research groups, reinforcing the notion that CD24 is highly expressed in TNBC tumor tissues, making it a potential surface marker and a promising target for TNBC treatment[33,34].

Therefore, to develop our ANCs, we strategically designed antibodies specifically targeting CD24 to enhance the efficacy and specificity of the treatment, minimizing off-target effects.

2.2. Design and synthesis of the linker and payload moieties

Current literature extensively documents that, while oxycisplatin exhibits robust stability in circulation, it can be reduced to cisplatin in the reductive environment of tumor sites. Given the ongoing clinical studies on various oxycisplatin derived drugs, we chose to attach the oxidized cisplatin axial ligand to a long-chain structure, serving as a connecting arm in the ANCs[35-37].

Furthermore, O^2-protected diazeniumdiolates have shown promising potential in the selective release of NO, and the propargyl protection mechanism is particularly effective for bioorthogonal activation. These compounds can release a high concentration of NO through a Pt-mediated bioorthogonal chemical reaction. Thus, our design consisted in integrating the NO donor to the oxidized cisplatin chain to obtain a conjugated small-molecule component. Supporting Information Figs. S2 and S3 depict the synthetic pathway of these molecules. Briefly, we obtained oxycisplatin (**1**) from cisplatin using a standard method[30]. We coupled *N*-Boc-protected 1,8-octanediamine with maleimide to obtain compound **3**, which contains a warhead capable of reacting with thiols, then coupled it with succinic anhydride to yield the carboxylic acid compound **4**. Then, we obtained diazeniumdiolate **2** by reacting *N*-Boc-piperazine with NO gas under high pressure followed by O^2-protection to separately yield the O^2-propargyl (**5a**) or -propyl (**5b**) protected derivatives[29]. Further reaction with succinic anhydride yielded the corresponding carboxylic acid derivatives **6a** and **6b**. Then, to facilitate coupling with oxidized platinum **1**, we synthesized the active esters **7a** and **7b**.

Subsequently, we successively coupled **7a** with oxidized platinum **1** and the carboxylic acid linker **4** to construct the coupled small-molecule **S**. To facilitate the investigation of its *in vitro* stability and kinetic properties, we mimicked the conjugation with an antibody by capping the warhead of small-molecule **S** with acetylcysteine, resulting in the formation of **CS**. Furthermore, to assess the impact of cisplatin and NO on the activity of the small molecule, we synthesized analog **S1**, which bore an O^2-propyl rather than O^2-propargyl group. **S1** could not be deprotected to release NO. In addition, we synthesized the O^2-propyl analog **S2** which did not contain the Pt(IV) moiety. We conjugated **S1** and **S2** were conjugated with an antibody to use as negative controls. Similar to CS, we synthesized **CS1** and **CS2.**

We discovered that **CS** exhibited favorable stability in rat plasma within a 4-h period (Supporting Information Fig. S4). This

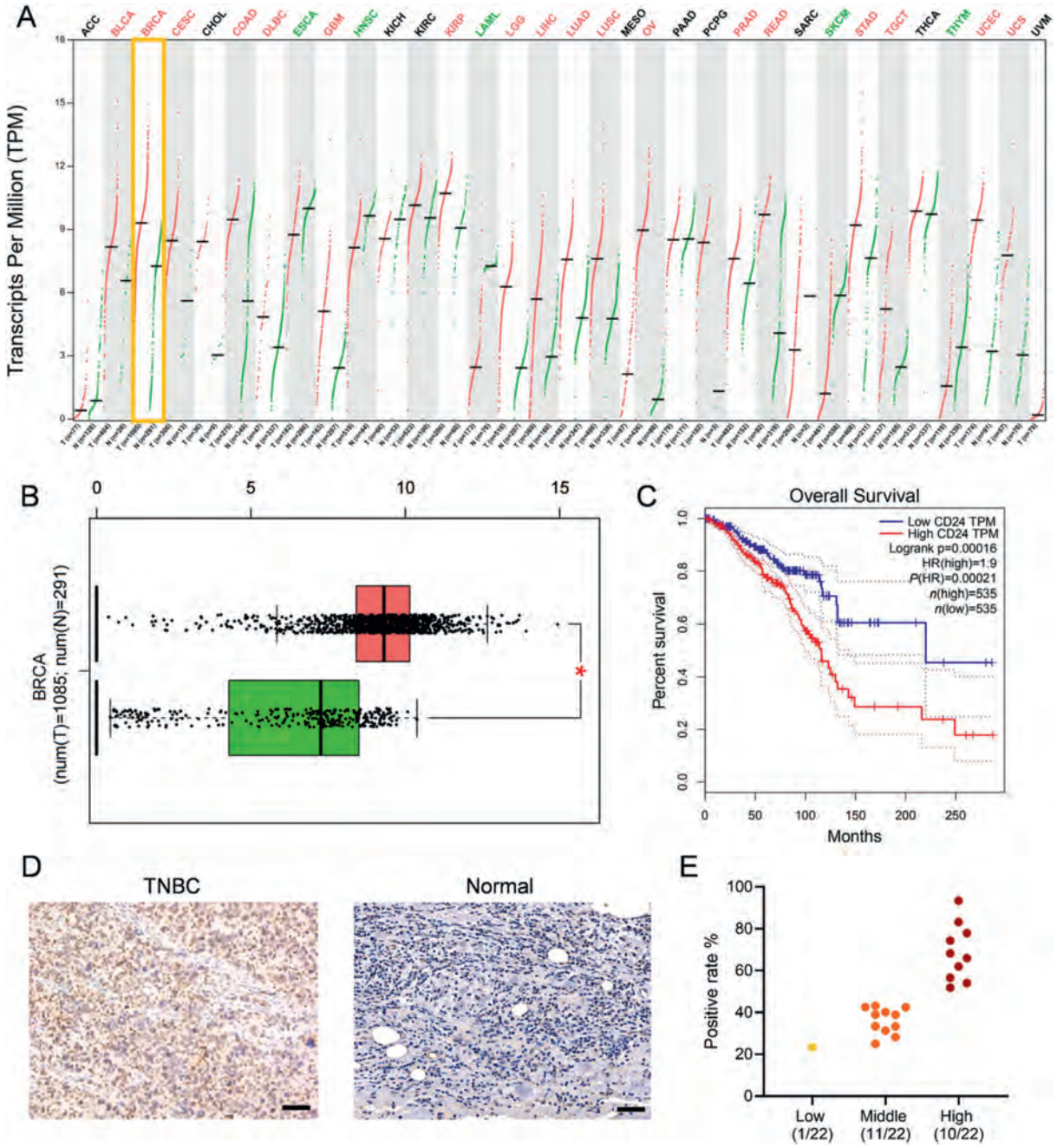

Figure 1 Clinical data analysis of CD24 expression and its correlation with patient prognosis. (A) Gene expression profile of CD24 in tumor samples and paired normal tissues (dot plot). Each dot represents a sample. In red are the cancer types with elevated CD24 expression levels relative to normal tissue. The *y* axis is $\log_2$ (TPM + 1). T: tumor tissue; N: normal tissue. Breast cancer is framed in yellow. (B) Box plot of CD24 expression levels in tumor tissue and normal tissue of patients with breast cancer. (C) Kaplan−Meier curves of breast cancer patients with high and low CD24 expression levels. Dotted lines represent 95% confidence intervals. $^*P < 0.05$. (D) Representative CD24 immunochemistry images of tumor tissue and paired normal tissue of TNBC patients. Scale bar: 50 μm. Other samples are in the Supporting Information (E) Statistics of samples with different CD24 expression levels. Each dot represents the positive rate of one sample. $n = 22$.

finding forms the foundation of indicating the stability of ANC in circulation and ensures its safety. Additionally, we confirmed its bioorthogonal catalytic kinetic characteristics in bioreductants and determined its approximate half-life (17 h) (Supporting Information Fig. S5). This result suggests that the small-molecule **CS** can be activated and reduced to cisplatin within the tumor microenvironment, thereby facilitating the subsequent bioorthogonal release of NO.

*2.3. Rational design and preparation of **HN03** from site-direct mutant cG7-SV and small-molecule **S***

With the conjugated small molecule in hand, we designed the corresponding monoclonal antibody. The site-conjugated product can be prepared *via* the addition reaction of the maleimide ring carried by small-molecule **S** with cysteine at the mutation site of the antibody cG7-SV. According to the research of previous

reports (Patent No. WO2024129756), we preliminarily selected LC-V211C, HC-A114C and HC-S239C as candidates for mutation design of CD24 antibody cG7. First, the Molecular Operating Environment (MOE) was used to analyze the surface residue exposure of the three sites[38]. The residue exposure levels were 16.77% for LC-V211C, and 51.31% for HC-A114C, and 25.44% for HC-S239C. Among these, the residue exposure level of HC-A114C was notably higher (>40%), which could potentially lead to the shedding of the loaded drug during blood circulation[39]. Therefore, we chose to proceed with the mutation regimen targeting LC-V211C and HC-S239C. We produced homology models of the mutant antibody cG7-SV and its progenitor cG7 using MOE (Supporting Information Fig. S6A). The modeling results revealed that these two mutations within the constant region of the antibody did not change the solvent exposure level at that location and negligibly affected its overall structural integrity (Fig. S6B). Furthermore, compared with the three commercially available antibodies MabThera®, Herceptin®, and Keytruda®, these mutations did not significantly alter the surface hydrophobicity or charge characteristics of the antibody, nor did they compromise its stability in aqueous environments (Fig. S6B and S6C). These findings, combined with our prior laboratory investigations of the internalization rate and antigen-binding efficacy of cG7-SV, assert that this antibody variant is suitable for ADC development.

We obtained monoclonal antibody cG7-SV at high purity through a series of purification steps after fermentation of N54 engineered cells cotransfected with the corresponding plasmids. As shown in Supporting Information Fig. S7, we purified cG7-SV purified using protein A chromatography and ultrafiltration. Sodium dodecyl sulfate−polyacrylamide gel electrophoresis (SDS−PAGE) showed that cG7-SV had a molecular weight of approximately 150 kDa, with smaller forms at 50 kDa and 25 kDa, consistent with IgG antibody characteristics. Subsequently, we linked small-molecule **S** to cG7-SV *via* a maleimide linker after exposing thiol groups using tris (2-carboxyethyl) phosphine hydrochloride (TCEP) and keeping them free with dehydroascorbic acid (DHAA). This resulted in the site-specific conjugate **HN03** (Fig. 2A). A BCA assay confirmed its concentration, showing an 89.3% recovery rate. Supporting Information Fig. S8 depicts the SDS−PAGE results after each step.

The hydrophobicity of ADCs typically increases with DAR. Hydrophobic interaction chromatography−high-performance liquid chromatography (HIC−HPLC) separates compounds and conjugates by hydrophobicity (with longer retention times for higher hydrophobicity). ADCs with small molecules coupled at various positions show multiple peaks and have DARs of 0−8, while site-specific ADCs theoretically show a single peak. Size-exclusion chromatography−HPLC (SEC−HPLC) separates by molecular weight, assessing purity. cG7-SV (naked antibody) and **HN03** (ANC) had similar molecular weights, with SEC−HPLC retention times of 7.732 min (96.96% peak) and 7.734 min (100% peak), respectively. In HIC−HPLC, naked anti-cG7-SV had a retention time of 12.315 min (100% peak), while that of **HN03** was 14.058 min (100% peak), indicating that the latter was more hydrophobic and homogenous. We determined the Pt content using inductively coupled plasma mass spectrometry (ICP−MS) and then calculated the DAR of the ADCs. The calculated conjugation ratio of cG7-SV to **S** was 3.82, which was very close to the theoretical value DAR = 4.

Flow cytometry showed that **HN03** could effectively bind to various cell lines (MDA-MB-468, SK-OV-3) with different levels of CD24, and also had a high level of binding to EMT-6-hCD24 and CHO-S-hCD24 cells overexpressing human CD24. However, it hardly bound to MDA-MB-231 and wild-type CHO-S cells with low CD24 expression, as shown in Fig. 2B and Supporting Information Fig. S9. This result suggests that **HN03** retains the targeting ability of the parent antibody cG7-SV, and confirms that these cells can be used for subsequent experiments.

To confirm the importance of the warhead molecule **S** in **HN03**, we prepared control conjugates **HN03-A** and **HN03-B** by conjugating the cG7-SV antibody with the control small molecules **S1** (O^2-propyl analog with Pt moiety) and **S2** (O^2-propyl analog without Pt moiety). The schematic structures and characterizations of control conjugates **HN03-A** and **HN03-B** appear in Supporting Information Fig. S10.

2.4. *In vitro bioevaluation of **HN03***

To evaluate the activation of **HN03**, we measured intracellular NO levels, which indicate that the prodrug has released cisplatin and NO in tumor cells. We incubated MDA-MB-468 cells with **HN03**, **HN03-A**, **HN03-B**, cG7-SV (all at 250 nmol/L), and **CS** (1 μmol/L, four times the antibody molar amount). Using the DAF-FM-DA probe, we found that **HN03** significantly increased intracellular NO, evidenced by distinct green fluorescence (Fig. 2C and D). This indicates that tumor cells uptake **HN03**, which then releases NO.

To ensure the **HN03** payloads are released at the tumor cells and assess its plasma stability, which is related to systemic toxicity in ADC drugs, we incubated 10 μmol/L **HN03** in human plasma for 72 h and assessed its ability to bind to tumor cells and release NO by flow cytometry. **HN03** (100 nmol/L) stably bound to MDA-MB-468 cells over 72 h (Fig. 2E and F). Similarly, NO levels, measured using the DAF-FM-DA probe, barely changed over 72 h. DAF-FM DA binds to NO and emits green fluorescence, which we analyzed using fluorescence microscopy and flow cytometry, respectively[40]. These results indicate that the linker and drug are stable in human plasma, which ensure the stable delivery of **HN03** to the target.

To understand the intracellular behavior of **HN03**, we tracked its distribution relative to lysosomes in MDA-MB-468 cells over time. We marked **HN03** with green fluorescent antibodies and lysosomes with red fluore-antibodies (Fig. 2G). Confocal microscopy revealed that at $t = 0$, **HN03** was bound only to cell surfaces. After 0.5 h of incubation at 37 °C, intracellular **HN03** fluorescence increased, and by 3 h, **HN03** was notably colocalized with lysosomes. These results indicate that **HN03** is transported to lysosomes after internalization and its payloads are released through lysosomal degradation.

Subsequently, we assessed the *in vitro* antitumor activity of **HN03**. The cytotoxicity of monoclonal antibodies alone is limited, and free small molecules can hardly target tumor cells, which limits their antitumor activity. In the conjugate **HN03**, the CD24 antibody delivers the toxic drug to tumor cells, theoretically enhancing the antitumor effect. Through prior validation, we demonstrated that the conjugate **HN03** can selectively bind to and internalize into breast cancer cells *via* CD24 antibody targeting, with intracellular **HN03** successfully activated to release elevated levels of NO. Building on these findings, we aim to validate whether the design of **HN03** effectively integrates the functional properties of antibodies and small molecules to achieve potent inhibition of breast cancer cells. Additionally, we seek to establish that the structural integrity of **HN03** is critical for its specific anti-

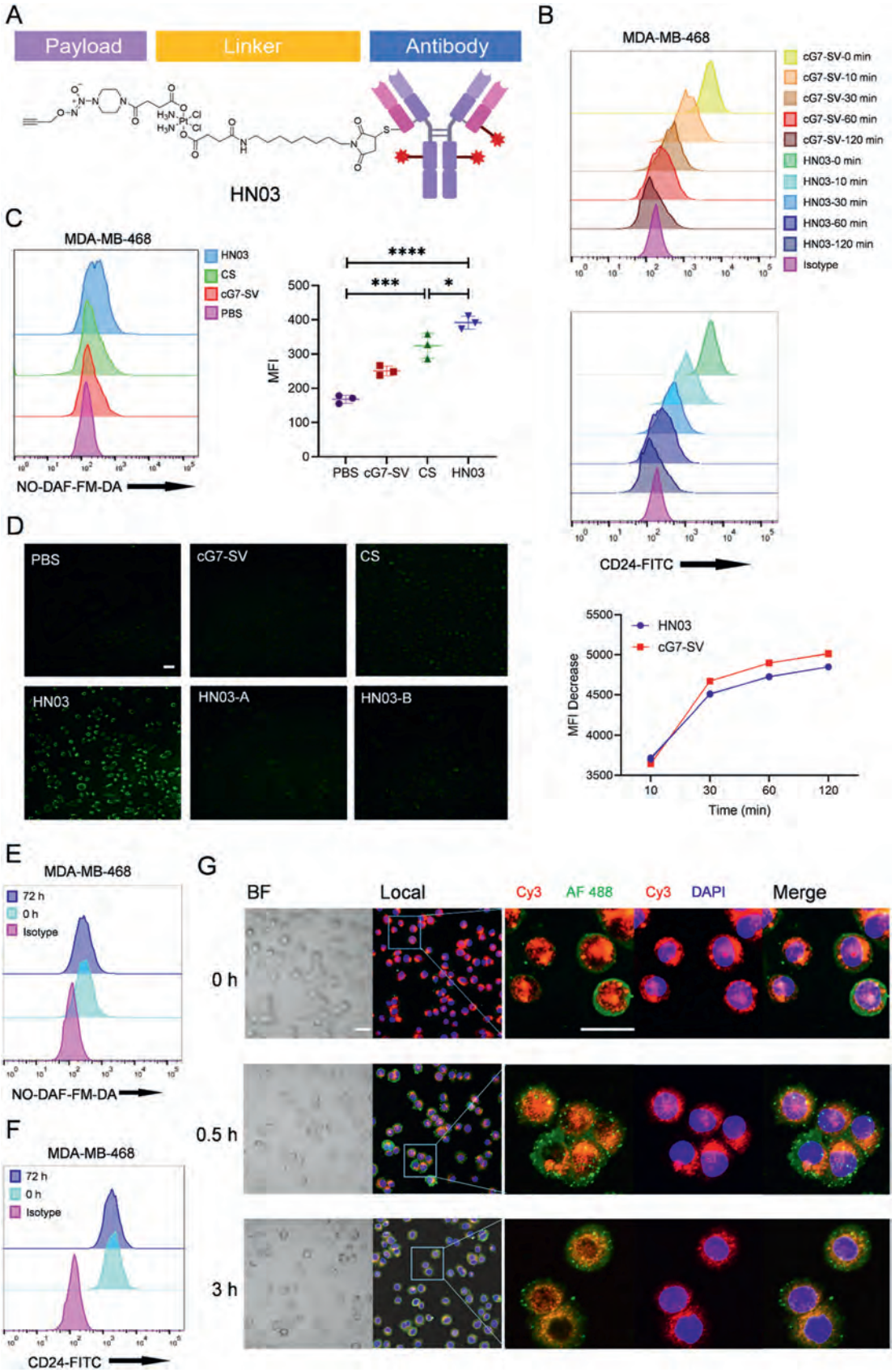

Figure 2 *In vitro* characterization of **HN03** internalization, plasma stability, and NO release. (A) Schematic diagram of the structure of **HN03**. (B) Variation curves of cell surface fluorescence intensity (flow cytometry) scent of **HN03** and cG7-SV on the cell surface after incubation in human plasma for various durations. Date are shown as mean ± SD ($n = 3$). (C) Intracellular fluorescence intensity (detected using the

breast cancer effects. To confirm this hypothesis, we first compared the inhibitory effect of **HN03** on TNBC cell proliferation with that of the naked antibody cG7-SV and the small-molecule **CS** through MTT experiments (Fig. 3A). At 1000 nmol/L, the conjugate **HN03** inhibited over 90% of the growth of MDA-MB-468 and EMT-6-hCD24 cells, with IC_{50} values of 216 and 382.8 nmol/L, respectively, outperforming the naked antibody and small molecule. However, it did not affect MDA-MB-231 and CHO cells. These results indicate that for TNBC cells with high expression levels of CD24, such as MDA-MB-468, the inhibitory effect of **HN03** on proliferation is dose-dependent, and the conjugate **HN03** exhibits better antitumor proliferation capability than the naked antibody cG7-SV and small-molecule CS, thereby selectively targeting tumor cells with high expression levels of CD24, thus demonstrating good CD24-targeting of **HN03**.

Moreover, the control conjugate **HN03-A** (O^2-propyl analog with Pt moiety) and **HN03**-B (O^2-propyl analog without Pt moiety) both had partial structural deletion, so theoretically the antitumor activity was limited. The small-molecule part of **HN03** exhibited a markedly superior antiproliferative effect to that exhibited by the control conjugates **HN03-A** (without NO donor) and **HN03-B** (lacking Pt prodrug) on MDA-MB-468 and EMT-6-hCD24 cells (Fig. 3C). It achieved over 90% inhibition with IC_{50} values of 206 nmol/L on MDA-MB-468 cells and 298.9 nmol/L EMT-6-hCD24 cells. This result underscores the necessity of both the Pt(IV) linker and NO donor in the prodrug **S** for selective antitumor activity. However, its impact on CHO-S-hCD24 cells, a normal hamster ovarian cell line overexpressing human CD24, was relatively low (under 20%), highlighting that the antitumor effectiveness of **HN03** is influenced by the tumor microenvironment with limited effects on normal cells. The anti-tumor effect of **HN03** is not only required by its targeting of CD24 on the surface of breast cancer cells. It also depends on the activation of **HN03**'s payload release mechanism by the high concentration of reducing substances in the tumor microenvironment.

Our literature review revealed that NO could promote protein nitrosylation and DNA damage, leading us to hypothesize that **HN03** induced tumor cell apoptosis by stimulating endoplasmic reticulum (ER) stress[41]. To evaluate the apoptotic effect of **HN03**, we incubated EMT-6-hCD24 cells with **HN03** (1 μmol/L), cG7-SV (1 μmol/L), and **CS** (4 μmol/L) for 72 h. We quantified apoptosis by counting annexin V-positive cells through flow cytometry (Fig. 3B). **HN03**-treated cells had an apoptosis rate of approximately 30%, while those of the cG7-SV- and CS-treated cells were below 20%. These findings indicate that **HN03** had a more potent apoptotic effect than cG7-SV and CS. To explore the apoptosis pathway, we quantified proteins related to ER stress using Western blot. As shown in Fig. 3D, **HN03** concentration-dependently increased the expression of proteins such as p-PERK, p-eIF2α, DDIT3, Bax, and Caspase 3, and decreased Bcl-2 expression. The antibody cG7-SV slightly upregulated the expression of ER stress-related proteins, while **CS** has a certain activation effect on the expression levels of apoptosis-related proteins. In summary, **HN03** appears to induce downstream endogenous cell apoptosis through the p-PERK−p-eIF2α−DDIT3 pathway, potentially relying on the combined action of cG7-SV and the small-molecule **CS** (Fig. 3E).

2.5. *In vivo bioevaluation of **HN03***

Based on *in vitro* experimental data, we established a human TNBC cell xenograft model by inoculating MDA-MB-468 cells into the right front limb axilla of BALB/c nude mice (Fig. 4A). When the tumor volume reached 100 mm^3, we randomly divided the mice into the following groups: Saline group, **HN03**-H group (10 mg/kg), **HN03**-L group (5 mg/kg), cG7-SV group (10 mg/kg), **CS** group (0.28 mg/kg), and cisplatin group (5 mg/kg). Considering the potent toxicity of the chemotherapeutic agent cisplatin, we administered it as the positive control at a dose of 5 mg/kg[42,43]. In contrast, given the low toxicity profile of the unconventional payload NO and its relatively high *in vitro* IC_{50}, we evaluated the conjugate at two dose levels: 5 mg/kg and 10 mg/kg. For comparison, the control monoclonal antibody cG7-SV and the small molecule **CS** were administered at equimolar concentrations corresponding to the higher dose group. The mice received the treatment twice a week, and we recorded tumor volume every two days. The tumor growth curves (Fig. 4B) show that the tumor volume increased rapidly in the saline group, with an average tumor volume of approximately 1400 mm^3 on Day 23, significantly larger than in the various treatment groups. The **HN03** high dose and cisplatin both significantly inhibited the growth rate of tumor tissue. The **HN03** low dose had a less pronounced inhibitory effect than the high dose but was still more effective than cG7-SV and **CS**. These results indicate that the conjugate **HN03** exhibits a superior antitumor effect to cG7-SV and **CS**.

Next, we assessed the antitumor efficacy of **HN03** at various doses in a mouse model with cisplatin as a positive control (Supporting Information Fig. S11). After 25 days, all treatment groups had lower tumor weights than the saline control group ($P < 0.001$), indicating the effectiveness of the treatments. Cisplatin demonstrated notable tumor suppression, with an average tumor weight of approximately 690 mg with a tumor inhibition rate of 60.87% (Fig. 4C and D). We used this as a benchmark for the efficacy of **HN03**. The low-dose **HN03** treatment resulted in an average tumor weight of approximately 820 mg. Notably, the high-dose **HN03** group exhibited the most significant reduction in tumor weight, averaging around 600 mg, with a tumor inhibition rate of 65.91%. Thus, the antitumor activity of **HN03** is dose-dependent, which is pivotal in evaluating its therapeutic window. Besides, high-dose **HN03** slightly surpassed the tumor suppression achieved by cisplatin (albeit nonsignificantly). By contrast, the naked antibody and small-molecule drug **CS** showed lower efficacy, with tumor weights of approximately 1010 and 1190 mg, respectively, and inhibition rates markedly lower than the high dose of **HN03** ($P < 0.001$).

DAF-FM-DA probe) in MDA-MB-468 cells treated with **HN03** (250 nmol/L), cG7-SV (250 nmol/L), or CS (1 μmol/L). Statistical analysis of mean fluorescence intensity: $*P < 0.05$; $***P < 0.001$. The results were analyzed by one-way ANOVA. Data are shown as mean ± SD ($n = 3$). (D) Fluorescence microscopy images of MDA-MB-468 cells treated with **HN03** (250 nmol/L), cG7-SV (250 nmol/L), **CS** (1 μmol/L), **HN03-A** (250 nmol/L), and **HN03-B** (250 nmol/L) in the presence of DAF-FM-DA to reveal NO. Scale bar: 50 μm. (E) NO release in MDA-MB-468 cells treated with **HN03** incubated in plasma at 37 °C for 0 or 72 h. (F) Binding capacity of **HN03** to MDA-MB-468 cells after incubation at 37 °C for 0 or 72 h in plasma, detected by flow cytometry. (G) Colocalization analysis of **HN03** (green) and lysosomes (red), marked with nuclei in blue. Scale bar: 50 μm.

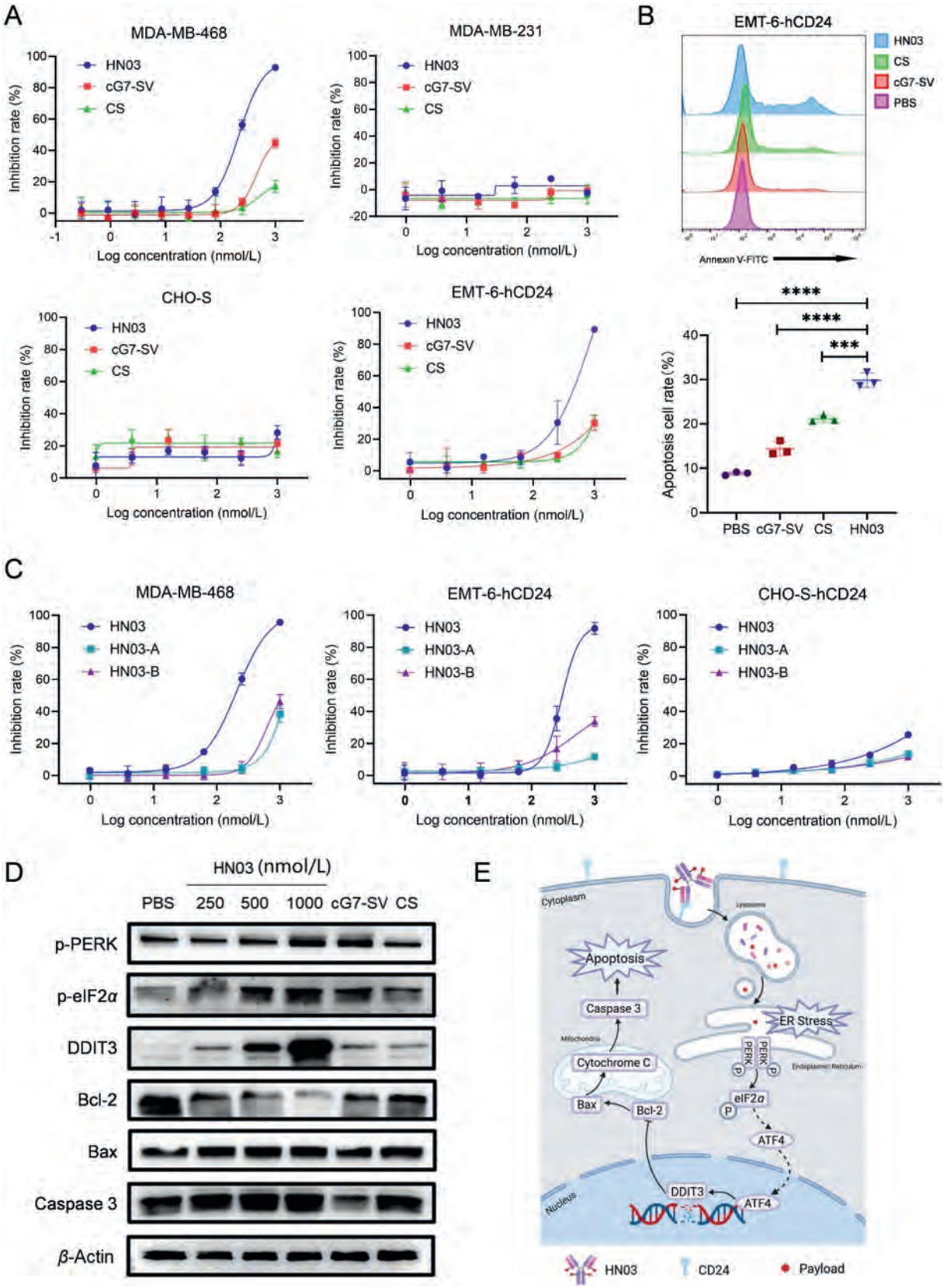

Figure 3 **HN03** inhibits proliferation of $CD24^{+}$ breast tumor cells and induces endoplasmic reticulum stress-induced apoptosis. (A) Inhibition curves of **HN03**, cG7-SV, and CS on the proliferation of MDA-MB-468, EMT-6-hCD24, MDA-MB-231, and CHO-S cells. The results were analyzed by one-way ANOVA. Date are shown as mean ± SD ($n = 3$). (B) Proportion of annexin V−positive cells after administration of **HN03** (1 μmol/L), cG7-SV (1 μmol/L), and **CS** (4 μmol/L) determined by flow cytometry. The right figure shows the quantified results. $^{**}P < 0.01$;

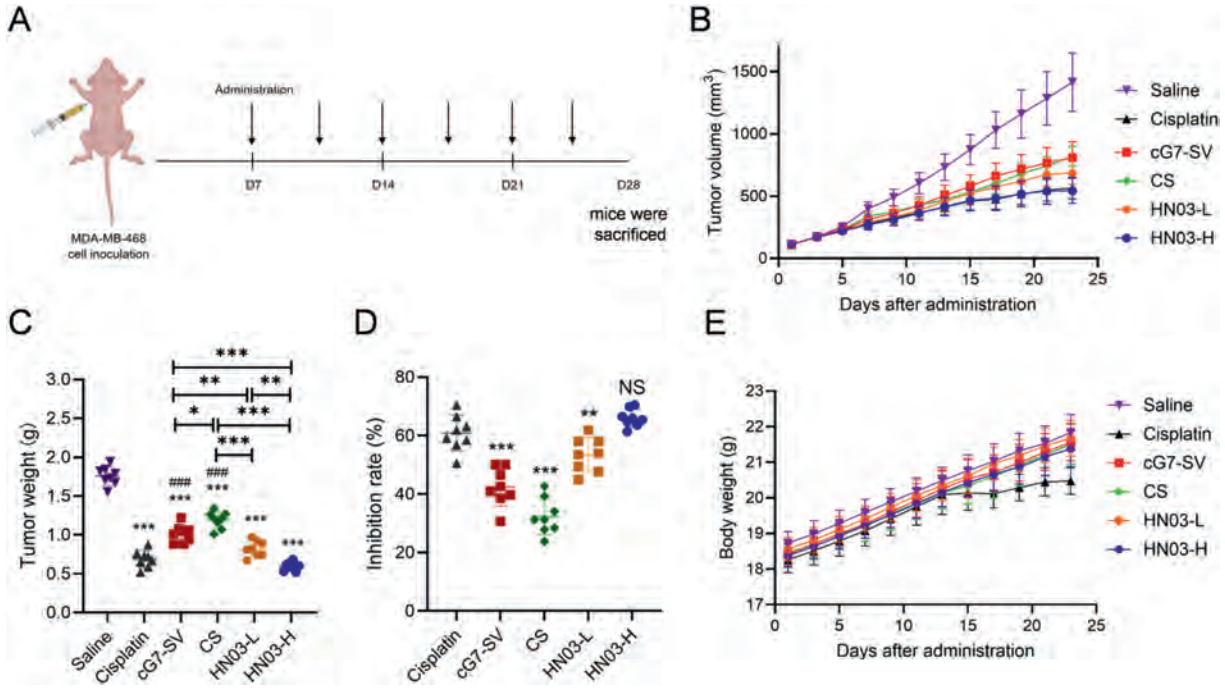

Figure 4 *In vivo* tumor inhibitory effect and safety of **HN03** in a mouse tumor model ($n = 8$). (A) Timeline of tumor model establishment and treatment. Nude mice received an injection of 1×10^7 MDA-MB-468 cells and, after 10 days, when the tumor reached 100 mm^3, they received a twice-weekly tail vein injection of the treatment. (B) Tumor volume growth curves. Data are shown as mean ± SD. (C) The final tumor weights in each treatment group. $^*P < 0.05$; $^{**}P < 0.01$; $^{***}P < 0.001$ *vs* saline groups or between indicated groups. $^{\#\#\#}P < 0.001$ *vs*. cisplatin group. The results were analyzed by one-way ANOVA. Date is shown as mean ± SD. (D) The tumor inhibition rate in each group. Compared with cisplatin group: $^{**}P < 0.01$; $^{***}P < 0.001$; NS: not significant. The results were analyzed by one-way ANOVA. Date are shown as mean ± SD. (E) Body weight curves of each treatment group. Date are shown as mean ± SD.

Further observation of the body weight (Fig. 4E) and general health of mice revealed an interesting safety profile. Cisplatin, a widely studied chemotherapy agent, is also a common positive control in mouse tumor models. Although its anticancer effect is well recognized, the clinical side effects of nephrotoxicity[44], neurotoxicity[45], ototoxicity[46], gonadal toxicity, gastrointestinal toxicity, muscular atrophy and anemia similar to those in the mouse model cannot be ignored. The complex mechanism of toxicity is most intuitively reflected in mouse models with rapid weight loss and decreased activity. Despite the similar tumor inhibition rates of cisplatin and high-dose **HN03**, after 13 days of continuous administration, cisplatin-treated mice exhibited signs of toxicity, such as reduced weight gain, decreased activity, and diminished appetite. In contrast, mice treated with **HN03**, irrespective of the dose, along with those in the cG7-SV and **CS** groups, showed no significant adverse effects, with a stable increase in body weight, indicating that **HN03** had a potentially safety profile than cisplatin.

In summary, the conjugate **HN03** effectively inhibited the growth of TNBC subcutaneous tumors, with a significantly better inhibitory effect than the naked antibody and precursor drug. Furthermore, **HN03** exhibited fewer side effects and better safety than cisplatin.

To investigate whether **HN03** could inhibit other types of breast tumors expressing high CD24 levels, we injected EMT-6-hCD24 cells into the fourth mammary fat pad of BALB/c mice, establishing a mouse mammary carcinoma *in situ* model overexpressing human CD24. We first conducted a preliminary experiment, which yielded results close to our expectations (Supporting Information Figs. S12 and S13): compared with the control (phosphate-buffered saline [PBS]), both **HN03** doses inhibited tumor growth without affecting body weight. However, the tumor inhibition effect was different within groups, while the tumor inhibition was relatively uniform in mice treated with **HN03** and doxorubicin (DOX; **HN03** + DOX). Therefore, we optimized the protocol and carried out the formal experiment. When the tumor volume reached 60 mm^3, we randomly divided the mice into the PBS group, **HN03**-H group (10 mg/kg), **HN03**-L group (5 mg/kg), and DOX group (3 mg/kg). Anthracyclines, particularly doxorubicin (DOX) as a representative agent, serve as first-line therapeutics for breast cancer due to their potent anticancer efficacy. However, their clinical application is often limited

$^{***}P < 0.001$. The results were analyzed by one-way ANOVA. Date are shown as mean ± SD ($n = 3$). (C) Inhibition curves of **HN03**, **HN03-A**, and **HN03-B** on the proliferation of MDA-MB-468, EMT-6-hCD24, and CHO-S-hCD24 cells. The results were analyzed by one-way ANOVA. Date are shown as mean ± SD ($n = 3$). (D) Expression changes of p-PERK-p-eIF2α-DDIT3 pathway and downstream apoptosis-related proteins in EMT-6-hCD24 cells after treating with **HN03** (0.25, 0.5, and 1 μmol/L), cG7-SV (1 μmol/L) and **CS** (4 μmol/L), obtained by Western blotting ($n = 3$). (E) Schematic diagram showing how **HN03** induces endoplasmic reticulum stress and apoptosis.

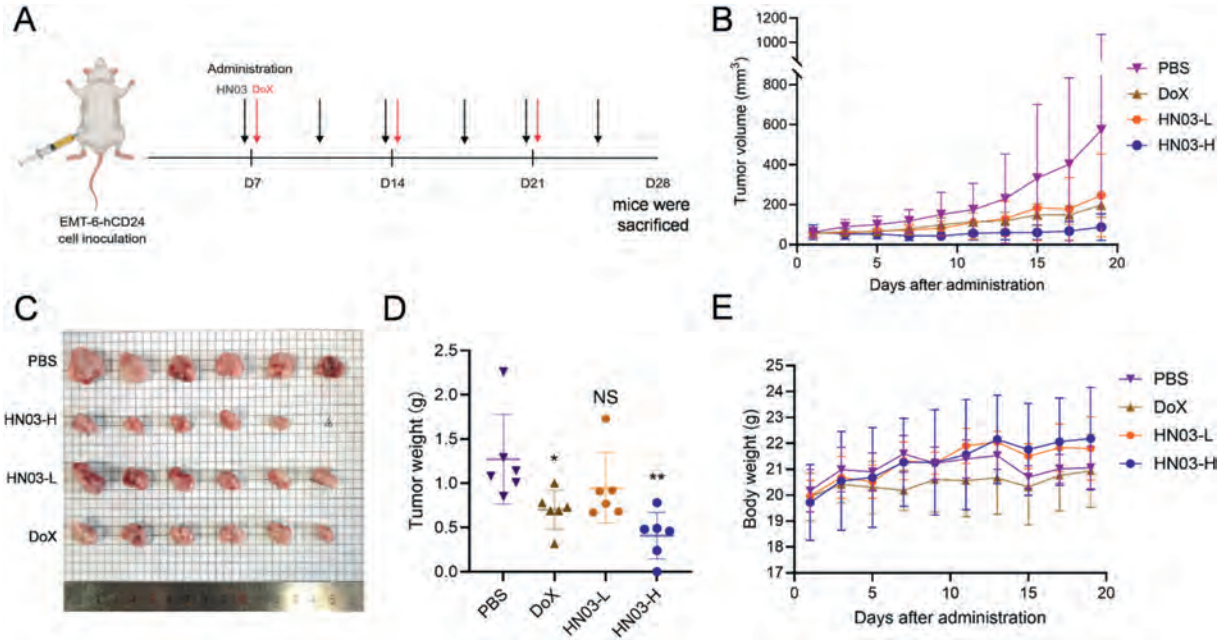

Figure 5 *In vivo* evaluation of antitumor effects of **HN03** on EMT-6-hCD24-transplanted mice ($n = 6$). (A) Timeline of tumor model establishment and treatment. BALB/c mice received a 1×10^6 EMT-6-hCD24 injection and, after 7 days, when the tumor volume reached 60 mm^3, the intraperitoneal treatment injections started. (B) Tumor volume growth curve. Data are shown as mean ± SD. (C) Photograph of tumors in each group. (D) The final tumor weights in each group. Compared with PBS group: $^*P < 0.05$; $^{**}P < 0.01$; NS: not significant. The results were analyzed by one-way ANOVA. Data are shown as mean ± SD. (E) Body weight curves for each group. Data are shown as mean ± SD.

by significant cardiotoxicity[47,48]. Based on preliminary experimental data and established dosing protocols for intraperitoneal administration in murine breast cancer models, DOX was administered at 3 mg/kg weekly[48,49]. Concurrently, **HN03** was evaluated at two dose levels, 5 and 10 mg/kg, to assess its therapeutic potential. We administered **HN03** twice a week, DOX once a week (based on preclinical dosing levels and frequency), and recorded tumor volumes every two days (Fig. 5A).

As shown by the tumor growth curve and final tumor weight histogram (Fig. 5B−D), the PBS group exhibited rapid tumor volume growth, with an average tumor volume of approximately 500 mm^3 on the 20th day, significantly larger than all treatment groups. Meanwhile, the positive control drug DOX achieved a 44.8% tumor inhibition rate ($P < 0.05$), establishing a comparative standard (Supporting Information Fig. S14). However, the treatments showed variable efficacy among individual mice, as detailed in the Supporting Information This variability underscores the nuanced response at lower dosages. Nevertheless, the **HN03** high dose markedly surpassed both the low-dose treatment and DOX, with a significant tumor inhibition rate of 67.9% ($P < 0.01$). The individual tumor growth curves clearly display the uniform and pronounced inhibitory effect of the high-dose regimen on tumor growth (Fig. S14F), highlighting the potent antitumor activity of **HN03** in this model. This sequential analysis reflects the dose-dependent efficacy of **HN03**, positioning the high-dose treatment as a highly effective therapeutic strategy against breast cancer, with clear potential advantages over traditional chemotherapy.

By further monitoring the body weight of BALB/c mice and weighing major organs (Fig. 5E), we found that, contrary to the DOX and PBS groups, the weight of the **HN03**-treated mice increased steadily and major organ weights were stable. By contrast, mice in the DOX group exhibited slow weight gain, significantly lower than the other groups (Fig. S14). Additionally, during the preliminary experiment, the DOX group underwent a sharp body weight drop and a dramatically higher death rate than group X, suggesting that this treatment method has severe side effects in animals. Mice in the PBS group showed reduced appetite and weight loss after 13 days of treatment, likely due to the rapid tumor growth affecting their normal physiological activities.

Considering the high invasiveness of this type of breast cancer and the side effects such as metastasis to the lung observed in clinical treatment with DOX, we performed HE staining of the lung tissues of mice in each group of the preliminary experiment. We observed significant heterogeneous areas in the lungs of mice in the DOX group, primarily around pulmonary vessels (Supporting Information Fig. S15A−S15D), consistent with the pathological characteristics of lung metastasis. By contrast, the high-dose **HN03** group displayed no such features, despite better tumor inhibition effects. Notably, the **HN03** + DOX group, while showing relatively uniform tumor inhibition, showed no lung metastasis. This confirms that **HN03** has can inhibit metastasis formation, which we hypothesize is due to the high concentration of NO inhibiting epithelial−mesenchymal transformation. In the third *in vivo* experiment, we preliminary verified this point by quantifying E-cadherin expression in tumor tissues from the PBS and **HN03**-H groups (Fig. S15E).

To comprehensively assess the safety profile of **HN03** and elucidate its therapeutic advantages over control conjugates, antibody−drug combinations, and small molecule therapies, we conducted an *in situ* anti-tumor efficacy study using the EMT-6-

hCD24 breast cancer model (Fig. 6). The experimental design incorporated multiple control groups, including cisplatin, monoclonal antibody cG7 (parent antibody of cG7-SV), cG7-HL2 (a first-generation antibody-NO donor conjugate utilizing HL2 payload), control conjugate **HN03-A**, and the combination therapy of cG7-SV with **CS**. Dosing regimens were established at 10 mg/kg for **HN03** and control antibodies/ADCs, 0.28 mg/kg for isomolar **CS** in combination therapy, and 4 mg/kg for cisplatin.

The cG7-HL2 conjugate, synthesized through a methodology consistent with our first-generation ANC **HN01**, exhibited characteristic peaks at 9.308, 9.766, 10.306, and 10.907 min corresponding to DAR values of 2, 4, 6, and 8, respectively, as determined by HIC−HPLC analysis. Quantitative assessment *via* area normalization revealed a DAR of 4.24 for cG7-HL2, comparable to that of **HN03** (Supporting Information Fig. S16A). Comparative analysis of plasma stability demonstrated that both cG7-HL2 and **HN03** maintained robust target cell binding capacity and NO release efficacy following 72-h plasma incubation, indicating comparable circulatory stability (Fig. S16B and S16C). However, **HN03** exhibited superior anti-proliferative activity against EMT-6-hCD24 cells relative to cG7-HL2 (Fig. S16D, Supporting Information Fig. S17).

As shown in Fig. 6A−D, **HN03** demonstrated remarkable antitumor efficacy, achieving tumor growth inhibition comparable to cisplatin (88.90% inhibition rate, average tumor weight of 258 mg), with complete tumor eradication observed in two subjects. cG7-HL2 exhibited moderate activity, while **HN03-A** and cG7-SV + CS showed limited efficacy.

To characterize the preliminarily pharmacokinetic profile and systemic toxicity of **HN03**, we implemented a comprehensive serum analysis protocol, incorporating pharmacokinetic parameter assessment and biochemical marker evaluation of liver function (ALT, AST), renal function (CREA, UREA), and hematological toxicity (WBC, PLT). The results showed that an extended half-life of ∼5 days (7528 min) for **HN03** in BALB/c mice, representing significant improvement over the ∼3-day half-life of first-generation ANC **HN01** (Fig. 6E). While cisplatin administration resulted in progressive weight loss and significant elevations in hepatic (ALT, AST) and renal (CREA, UREA) markers, **HN03**-treated animals maintained physiological parameters comparable to saline controls, demonstrating favorable safety margins (Fig. 6F). Furthermore, **HN03** mitigated the acute neutropenia commonly associated with commercial ADCs (including Trodelvy® and Enhertu®), maintaining WBC and PLT counts within normal ranges while sustaining potent anti-tumor activity.

In addition, the addition of high concentration of NO in our design not only plays an anti-tumor role, but also promotes the increase of intracellular cyclic guanosine phosphate (cGMP) levels by activating soluble guanylate cyclase (sGC), leading to vascular smooth muscle cell relaxation and vascular dilation. Studies have shown that by releasing NO in the tumor area, promoting the vascular normalization of the tumor microenvironment helps to increase the sensitivity of tumor cells to drugs, which promotes the invasion of Pt drugs at the tumor site.

The therapeutic efficacy of **HN03** is further enhanced by its NO-mediated mechanisms, which extend beyond direct anti-tumor effects. Through sGC activation and subsequent cGMP elevation, **HN03** may induces vascular smooth muscle relaxation and promotes tumor vascular normalization, potentiating drug delivery and enhancing tumor cell sensitivity to platinum-based therapeutics[50]. ICP−MS analysis of tumor tissue revealed that **HN03** facilitated > 2-fold greater platinum accumulation compared to the control conjugate (Supporting Information Table S1), validating our molecular design strategy and demonstrating effective NO-mediated enhancement of drug delivery.

Collectively, these findings demonstrate the superior safety profile and therapeutic potential of **HN03** across multiple dimensions, macroscopic tumor inhibition and weight maintenance, and microscopic evaluation of organ function and hematological parameters. These results underscore **HN03**'s potential as a novel ADC platform that optimizes therapeutic delivery while minimizing off-target effects, representing a significant advancement in targeted cancer therapy.

2.6. *Exploration of synergistic mechanism*

We collected tumor tissue from three mice in the PBS and **HN03**-H groups from the above experiments and sent them for transcriptome sequencing to investigate differences in gene expression. Due to objective constraints in the sequencing conditions, the tumor tissues submitted for analysis were relatively large individuals from each group. Principal component analysis did not clearly distinguish the two groups of samples (Supporting Information Fig. S18), but one **HN03**-H sample (**HN03**-3), which had undergone prominent tumor inhibition, showed significant differences with the PBS group.

We identified and counted respectively the number of upregulated and downregulated genes based on significant differential criteria (more than 2-fold change in gene expression and q-value ≤ 0.05). Compared with the PBS group, the **HN03**-H group had three significantly upregulated genes and nine significantly downregulated ones (Fig. 7A). The volcano plot of differential genes displays the SYMBOL names of the top 10 differentially expressed genes (Fig. 7B). The similarity-based clustering analysis of genes in the PBS and **HN03**-H groups revealed that sample **HN03**-3, which had undergone significant tumor inhibition, formed a distinct cluster, while the PBS group formed another cluster. **HN03**-1 and **HN03**-2, which showed relatively less tumor inhibition, grouped together. Overall, we found 12 differentially expressed genes (Fig. 7C). Among these, Car6, Ddit3, and Trib3 were upregulated, while Sema3e, Arg1, Wfdc17, Ccl6, Ccl9, Sfrp4, Lyz1, Rgs13, and Retnla were downregulated. Notably, the downregulation of Arg1 and Retnla is associated with the regression of M2 macrophage phenotype in the tumor. M2 macrophages promote tumor development. The upregulation of gene DDIT3 is associated with breast tumor cell apoptosis and DNA damage caused by ER stress, which is consistent with the apoptosis pathway verification results of the above *in vitro* antitumor activity experiments. Other genes are related to the inhibition of tumor epithelial−mesenchymal transition and other antitumor factors. For example, the most significantly downregulated CCL6 gene can not only inhibit the recruitment of M2 macrophages, but also inhibit tumor metastasis through the CCL6−CCR1 axis[51].

Tumor-associated macrophages come in two main types: M1 (classical) and M2 (alternative). M2 macrophages release anti-inflammatory factors, aiding tumor growth and immune suppression[52]. CD206 is a key marker for M2 macrophages. Using the Cy3 dye, we labeled M2 macrophages in tumor tissues (Fig. 7D) and observed that there were more M2 macrophages in the tumor tissues of the PBS and DOX groups than those in the **HN03** group. The tumor inhibition effect of the **HN03** low-dose group was worse than that of the **HN03** high-dose group, and M2 macrophage infiltration was more in the PBS and DOX groups than that

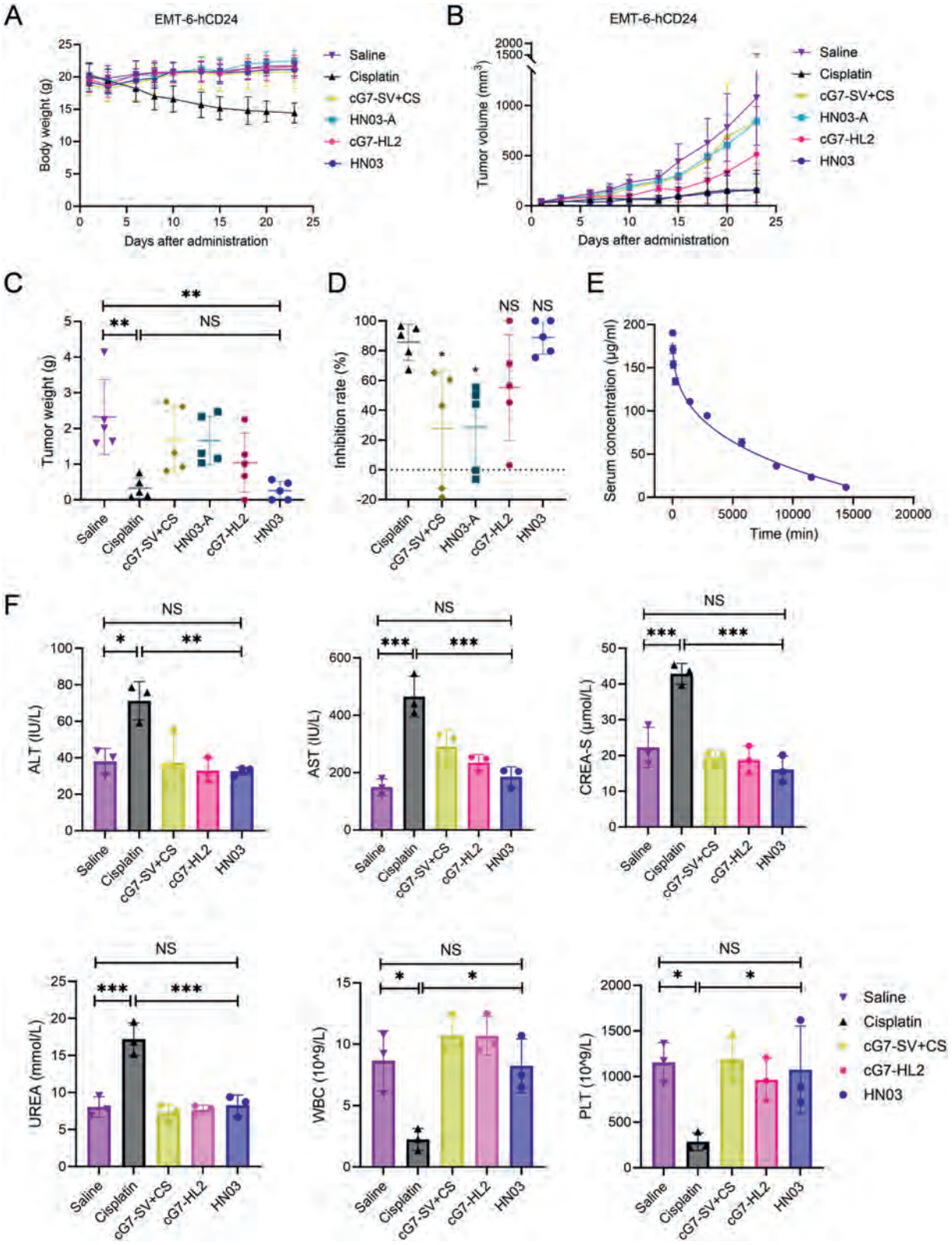

Figure 6 *In vivo* evaluation of **HN03** on EMT-6-hCD24-transplanted mice ($n = 5$). (A) Body weight curves for each group. Data are shown as mean ± SD. (B) Tumor volume growth curve. Data are shown as mean ± SD. (C) The final tumor weights in each group. Compared with saline group: $^{**}P < 0.01$; NS: not significant. The results were analyzed by one-way ANOVA. Data are shown as mean ± SD. (D) The tumor inhibition rate in each group. Compared with cisplatin group: $^{*}P < 0.05$; NS: not significant. The results were analyzed by one-way ANOVA. Data are shown as mean ± SD. (E) Plasma pharmacokinetic curve of HN03 in BALB/c mice. (F) Liver function (ALT, AST), renal function (CREA, UREA) and hematotoxicity (WBC, PLT) index of each group. $^{*}P < 0.05$; $^{**}P < 0.01$; $^{***}P < 0.001$; NS: not significant. The results were analyzed by one-way ANOVA. Data are shown as mean ± SD.

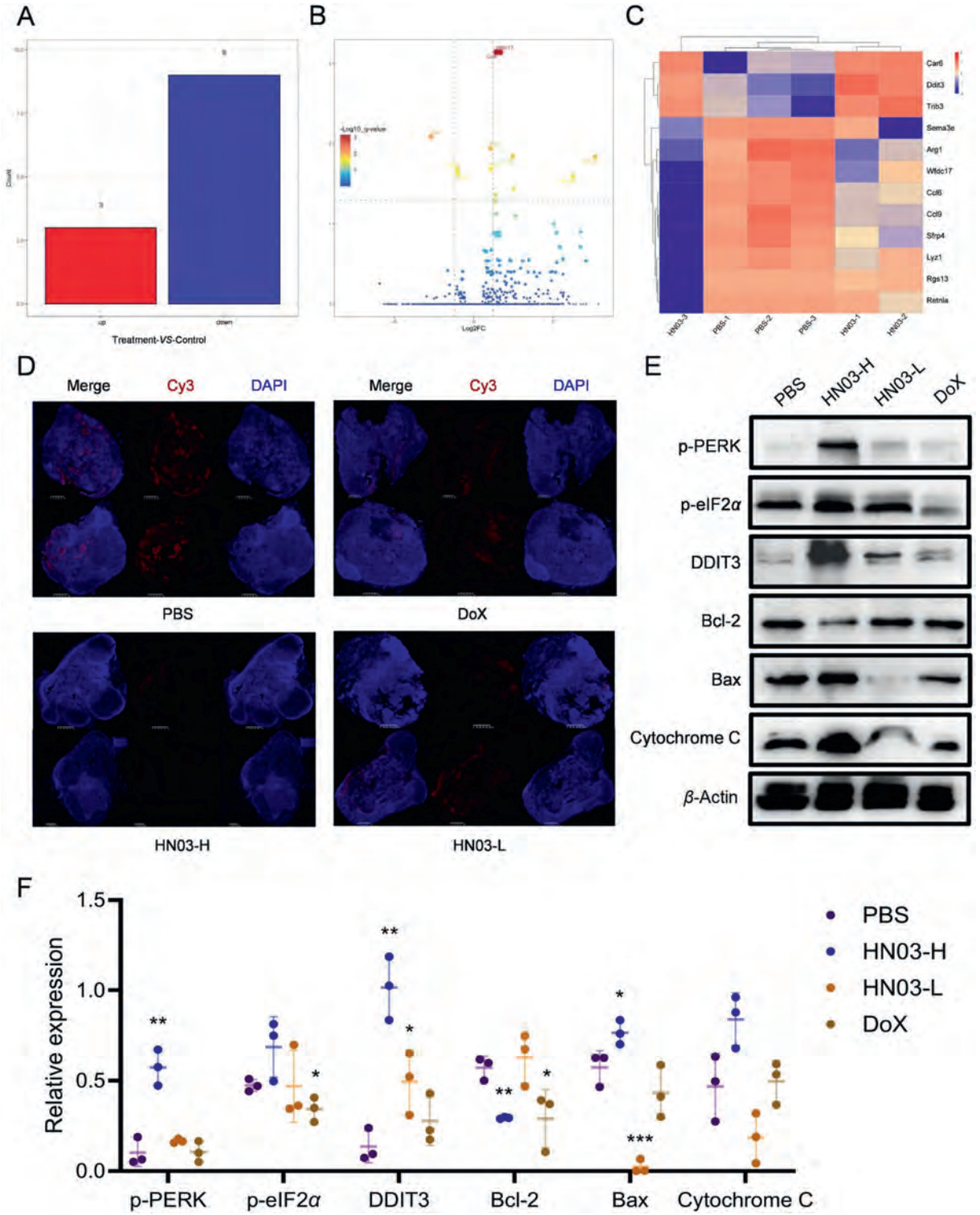

Figure 7 Effects of **HN03** administration on tumor transcriptome, protein expression, and immune cell infiltration. "Control" represents the control sample, "Treatment" represents the treated sample, and "Up/Down" indicates the upregulation or downregulation of genes the treated sample compared with the control. (A) Counts of upregulated and downregulated genes in the treated sample compared with the control sample. (B) Volcano diagram of differentially expressed genes. The size of the dots represents the degree of significance of genetic differences. (C) Differential gene clustering map. The $\log_{10}(\text{FPKM} + 1)$ value was used for clustering. High-expression genes appear in red and low-expression genes appear in blue. (D) Panoramic scan of immunofluorescence staining of M2 macrophages in tumor tissue sections of each group ($n = 2$). The CD206 protein, an M2 macrophage marker, was labeled with the red Cy3 dye. The below graphs of HN03-H group and the above graphs of HN03-L group: scale bar: 100 μm, others: scale bar: 200 μm. (E) ER stress- and apoptosis-related protein expression levels in tumor tissues in each group, obtained by Western blotting. (F) Quantification of the protein expression bands. The results were analyzed by one-way ANOVA. Compared with PBS group: $^{*}P < 0.05$; $^{**}P < 0.01$; $^{***}P < 0.001$. Data are shown as mean ± SD.

in the **HN03** groups. Additionally, the **HN03**-L group had more M2 macrophages and larger tumors than the **HN03**-H group. This result aligns with transcriptome sequencing, suggesting that **HN03** reduces M2 macrophage infiltration in tumors. Further analysis of M1-type macrophage infiltration showed that all groups except **HN03**-H had similar M1-type macrophage infiltration levels in tumor tissues, while the **HN03**-H dose group displayed high local infiltration (Supporting Information Fig. S19). Therefore, we speculate that **HN03** can affect the infiltration of M2-type macrophages in tumors, and the change of infiltration depends more on phenotype transformation than on direct killing.

Transcriptome sequencing revealed an upregulation of the ER stress- and DNA damage-related gene DDIT3 in the **HN03**-H group. *In vitro* experiments also indicated that **HN03** induces tumor cell apoptosis through ER stress. Therefore, **HN03** likely induces tumor cell apoptosis in mice by stimulating ER stress. As shown in Fig. 7E and F, the Western blot analysis of EMT-6-hCD24 tumor tissue samples showed significantly higher expression of ER stress-related proteins (p-PERK, p-eIF2α, DDIT3) and the proapoptotic protein Bax in the **HN03**-H group than in the PBS group. Conversely, the expression of the antiapoptotic protein Bcl-2 was lower in the **HN03**-H group, confirming the presence of ER stress-induced apoptosis. The **HN03**-L group exhibited slightly elevated ER stress-related protein levels, but no significant differences in apoptosis-related proteins, possibly explaining its weaker antitumor effect. The DOX group showed some differences in apoptosis-related proteins, albeit less pronounced than those in the **HN03**-H group. In summary, **HN03** induces endogenous cell apoptosis through the p-PERK−p-eIF2α−DDIT3 pathway *in vivo*, with a more significant effect at higher doses.

ADCs represent a groundbreaking advancement in the treatment of TNBC, combining antibody targeting specificity with small molecule cytotoxicity to precisely eliminate target cells[33,53]. Despite their promise, the high cytotoxicity of traditional ADC payloads often causes off-target toxicity and limit the therapeutic window[54]. In response, researchers have shifted focus toward low-toxicity payloads and increased DAR, striving to match or surpass the efficacy of conventional ADC[55]. Inspired by the promising effects of elevated NO levels in tumor biology and based on our previous work, we developed a novel ANC[56]. In this work, we refined the structure of the linker, optimizing its activity while minimizing toxicity.

CD24 is a surface marker for various tumor cells and was suspected to be associated with tumor development. Our bioinformatics analysis confirmed the high CD24 expression in breast cancer, particularly in TNBC, making it a potential prognostic tool for breast cancer patients. In this work, immunohistochemistry analysis revealed elevated CD24 levels in TNBC patient tissue samples, reinforcing CD24 as a promising target for TNBC treatment[57].

Site-specific conjugation technology became a significant trend in ADC drug development; it allows the design of drugs with uniform coupling sites and DAR values, thereby improving pharmacokinetic properties and therapeutic indices[58]. Employing an innovative engineered cysteine site-specific conjugation technology, the maleimide ring on the small molecule was conjugated to the mercaptan bond at the cysteine mutation site of the antibody by addition reaction, we designed an ADC specifically targeting TNBC cells overexpressing CD24. We developed a CD24 site-specific mutant monoclonal antibody, cG7-SV, with excellent antigen targeting ability and selectivity for CD24-positive tumor cells. We chose two specific mutation sites, heavy chain serine 239 (HC-S239) and light chain valine 211 (LC-V211), confirmed that the mutant antibody cG7-SV retained the structural and functional integrity of its parent antibody using molecular dynamics simulations.

Leveraging engineered cysteine site-specific conjugation technology, integrating a bioorthogonal self-activation strategy, and utilizing the gaseous signaling molecule NO as the payload, are the innovative features of this work. Accordingly, we successfully prepared the ADC drug **HN03** and characterized its physicochemical and biological properties. HIC−HPLC and SEC−HPLC results indicated that **HN03** was more hydrophobic than the naked antibody, without being susceptible to aggregation in aqueous solutions or antibody structure disruption. **HN03** exhibited good uniformity, consistent with typical site-specific conjugates. Quantitative analysis confirmed a DAR of 3.82, aligning with the theoretical design allowing the coupling of four small molecules. Cellular binding experiments demonstrated that **HN03** effectively targeted $CD24^+$ TNBC cell lines, including MDA-MB-468, and other $CD24^+$ cells, showcasing its remarkable selectivity.

To explore the *in vivo* anticancer effects of **HN03**, we established a human TNBC MDA-MB-468 cell xenograft model. High and low doses of **HN03** (10 and 5 mg/kg) both inhibited tumor tissue growth, surpassing the antitumor effect of the naked antibody cG7-SV (10 mg/kg) and the small-molecule **CS** (0.28 mg/kg) administered alone. The antitumor rate of the positive drug cisplatin (5 mg/kg) was slightly lower than that of the high **HN03** dose, albeit not significantly. Notably, cisplatin caused significant weight loss in mice, indicating toxicity, while **HN03** administration resulted in stable weight gain, suggesting good tolerance.

Considering the excellent CD24 targeting ability of **HN03**, we extended our investigation to an *in situ* breast cancer model overexpressing human CD24 (EMT-6-hCD24 cells) to assess its *in vivo* efficacy. With a 67.9% tumor reduction rate and tumor metastasis inhibition, the high **HN03** dose exhibited antitumor effects superior to those of the positive control drug DOX. Besides, neither the high nor the low **HN03** doses significantly affected body and organ weight. Transcriptome sequencing of tumors from the **HN03**-H group revealed significantly downregulated M2-type macrophage marker genes and upregulated ER stress-related indicator genes. Subsequent validation through immunofluorescence and Western blot testing confirmed the ability of **HN03** to induce a phenotypic shift in macrophages, significantly reducing M2-type macrophage infiltration in tumor tissues. This finding aligns with previous research on the impact of the parental antibody cG7 on immune cell infiltration. Additionally, **HN03** consistently induced ER stress and apoptosis in tumor cells *in vivo*, with higher **HN03** doses enhancing its antitumor activity and uniformity, suggesting a broader therapeutic window.

However, it is essential to note that this study solely assessed the antitumor effect of **HN03** and conducted preliminary exploration of its antitumor mechanism. Further research is warranted to investigate systemic toxicity, pharmacokinetic properties, and impact on the survival of tumor-bearing mice. Since the antibody used for **HN03** is of the IgG1 subtype, it may exert its antitumor activity by inducing antibody-dependent cell-mediated cytotoxicity, complement-dependent cytotoxicity, and antibody-dependent cellular phagocytosis. Subsequent studies should explore these effects and consider their retention or removal based on the strength of *in vivo* antitumor efficacy and systemic toxicity. Given the promising outcomes of combining PD-1 monoclonal antibodies with chemotherapy as neoadjuvant therapy and the

potential complementary role of the PD-1 pathway in CD24-positive TNBC, adjusting the dosing regimen to explore the therapeutic efficacy of **HN03** in combination with PD-1 monoclonal antibodies are worth considering.

TNBC is one of the most challenging subtypes of breast cancer; it lacks ideal molecular targets, has limited treatment options, and often displays high recurrence rates[5,59]. Here, we developed a novel ANC bearing a bioorthogonal self-cleavable linker, named **HN03**. As the first bioorthogonal ANC, it specifically targets TNBC cells expressing CD24. The exceptional selectivity and safety of **HN03** not only enhance tolerability but also improve prognosis and quality of life. Additionally, incorporating Pt(IV) as a bioorthogonal self-cleavable linker enhances the expandability of the payload, offering novel perspectives for the design of other ADCs. In fact, our research group also used Herceptin® to randomly conjugate small-molecule **S** and conduct a simple MTT verification, and found that it inhibited the proliferation of human epidermal growth factor receptor-2 (HER-2)-positive tumor cell lines. Furthermore, the mechanistic insights gained from this study reveal how **HN03** utilizes ER stress to induce apoptosis, improving our understanding of effective TNBC targeting. Furthermore, exploring the tumor microenvironment would help further enhance the effectiveness of **HN03**. In summary, this study paves the way for the future of TNBC treatment. The innovative design, good safety profile, and synergistic mechanism of **HN03** position it as a leader in effective TNBC treatment options. The potential to improve patient outcomes, coupled with its ability to selectively target CD24-expressing TNBC cells, underscores the significance of this research, and sets the stage for further clinical development, ultimately bringing a brighter future for TNBC patients.

3. Conclusions

In conclusion, we designed a site-specific conjugate **HN03**, consisting of a cysteine-engineered CD24 antibody and a bioorthogonal catalysis-based NO donor mediated by Pt(IV). With good antigen-binding ability and plasma stability, **HN03** specifically targets CD24-positive TNBC cells, and can be internalized to release cisplatin and high levels of NO. It significantly inhibits the growth of subcutaneous and *in situ* transplanted tumors with good safety, and induce the polarization phenotypic transformation of tumor infiltrating M2 macrophages.

4. Experimental

4.1. Study approval

All animal experiments and animal care performed in accordance with guidelines of the Provision and General Recommendation of Chinese Experimental Animals in China. The experimental protocols were approved by the Animal Research and Care Committee of China Pharmaceutical University (No. 2023-04-003) and in compliance with the National Institutes of Health guidelines for the ethical treatment of animals. All the clinical samples used in the paper meet the ethical requirements of Nantong Third People's Hospital, Affiliated Nantong Hospital 3 of Nantong University (EL2024004).

4.2. Analysis of database

The GEPIA platform (available at http://gepia.cancer-pku.cn) is an advanced tool that integrates RNA sequencing data from TCGA and GTEx databases. This integration allows for efficient comparison of gene expression in tumor and normal tissues. Additionally, it offers insights into the correlation between gene expression and patient survival in various cancers. On visiting the GEPIA website, one can choose the "Expression DIY" module. By selecting "profile" from the menu, inputting "CD24" as the gene of interest, setting the $\log_2$FC to 1, and adjusting the q-value to 0.01, users can generate a specific box plot. Furthermore, the platform facilitates survival analysis. By selecting the "survival analysis" module, entering "CD24", choosing "overall survival", setting a 50% group cutoff, and focusing on "BRCA" (breast cancer), users can conduct a detailed survival analysis based on TCGA breast cancer data.

4.3. Immunohistochemistry

Tissue samples from TNBC (triple-negative breast cancer) patients, who provided informed consent for the experiment, were initially fixed in 4% paraformaldehyde for 24 h. Subsequently, these samples were embedded in paraffin and sectioned into 5 μm slices. The slices were then baked at 60 °C and placed in a tissue tank. They underwent a xylene soak followed by hydration, ensuring the samples remained moist throughout the process. The sections were fully immersed in EDTA antigen repair solution (Beyotime P0085), heated to maintain a gentle boil for 15−20 min. Once cooled to r.t, the sections were sequentially soaked in double distilled water and PBS. To quench endogenous peroxidase activity, the sections were treated with a 3% hydrogen peroxide solution, followed by a PBS soak. A hydrophobic barrier was drawn around the tissue using an immunohistochemistry pen. Inside this barrier, 5% goat serum (diluted in PBS) was applied to completely cover the tissue, and the sections were blocked at r.t for 1 h. After discarding the blocking solution, a mouse anti-human CD24 antibody (1:1000 Proteintech 67627) diluted in 1% goat serum was applied as the primary antibody and incubated overnight at 4 °C. The sections were then washed in PBST solution with shaking and dipping. A HRP-labeled goat anti-mouse IgG antibody (1:1000 Proteintech SA00001-1), diluted in 1% goat serum, served as the secondary antibody and was incubated for 3 h at r.t, followed by another PBST wash. DAB staining solution (Beyotime P0202) was added to the sections, protected from light for 3 min, and then gently rinsed with tap water. Hematoxylin staining solution (Sangon Biotech E607317) was applied for counterstaining for 1 min, followed by a gentle tap water rinse. Subsequently, the sections underwent gradient dehydration using ethanol and xylene, from low to high concentrations, were dried, and then mounted with neutral resin. The prepared slides were examined and photographed using an upright microscope. The resulting immunohistochemistry images were analyzed for positivity using ImageJ software.

4.4. Design of cG7-SV

A chimeric antibody targeting CD24, named cG7, had been previously developed, demonstrating effective targeting capabilities. For the purpose of crafting antibody−drug site-directed conjugates, it was necessary to modify and mutate cG7. The initial step involved conducting homologous modeling of cG7 using the "antibody modeler" function within the MOE (Molecular Operating Environment) software. This process included an analysis of the antibody's solvent exposure and amino acid residues using MOE's "Properties" module. Additionally, the distribution of

hydrophobic and charge properties on the antibody's surface was examined using the "Patch Analyzer" module. Guided by the simulation results from MOE, specific mutations were introduced into the cG7 antibody. At position 239 of the cG7 heavy chain, a serine (TCA) was mutated to cysteine (TGC) using overlap-PCR. Similarly, in the light chain, a valine (GTC) at position 211 was mutated to cysteine (TGC). These modifications resulted in the creation of cG7-SV, a CD24 monoclonal antibody with strategically engineered cysteine residues, optimizing it for ADC development.

4.5. Purification of cG7-SV

The collected fermentation broth supernatant and the reagents required for purification were filtered through a 0.22 μm filter membrane and placed on ice for later use. The Protein A column was slowly rinsed with double distilled water and PBS. The loading flow rate was controlled so that the supernatant flowed through the protein A column at a rate of 1 mL/min, and the effluent was collected to prevent the antibody from hanging on the column. After loading, rinsed the column with PBS to remove impurities. Add eluent for elution, collect the outgoing eluate and immediately neutralize it with neutralization solution to pH 7.0, 4 °C storage. Rinse the column with PBS, double distilled water, and 20% ethanol sequentially, and finally fill the column with 20% ethanol and store at 4 °C. The collected eluate was ultrafiltered and concentrated with an ultrafiltration tube with a molecular weight cut-off of 50 kDa, and the solution system was replaced with PBS for short-term storage at 4 °C or long-term storage at −80 °C.

4.6. Antigen-binding capacity of cG7-SV

The enzyme strip was activated by UV lamp irradiation, and the antigen (hCD24-GST) was diluted to 0.5 μg/mL with $NaHCO_3$ buffer. Added 100 μL of diluted CD24 antigen per well and coated overnight at 4 °C. The antigen was discarded, the microplate was put into an ELISA plate washer and washed with PBST shaking, 200 μL of 5% skim milk was added to each well, and the plate was blocked at 37 °C for 2 h. Washed with PBST, added 100 μL of gradient concentrations of cG7 and cG7-SV as primary antibodies (0.008−2.5 nmol/L, diluted with 2% skim milk), set up 3 replicates at each concentration, and set up 2.5 nmol/L human IgG1 unrelated antibody as an isotype control, and incubated at 37 °C for 2 h. Washed with PBST and added 100 μL of HRP-goat anti-human IgG antibody (1:20,000, Proteintech SA00001-17, diluted with 2% skim milk) per well and incubated at 37 °C for 1 h. Washed with PBST, added 100 μL of TMB chromogenic solution per well, and reacted at r.t in the dark for 15−20 min until obvious blue appears. Stop solution was added to each well, absorbance at 450 and 630 nmol/L were read with a microplate reader (OD_{450}, OD_{630}), and the values of OD_{450}−OD_{630} were calculated, and the EC_{50} was plotted and calculated by Prism 9.0 software.

4.7. Internalization of cG7-SV

Pipetted 100 μL of cG7-SV and added 7.5 μL of NaHCO3 solution to adjust the pH to 8.5−8.9. Added 6.35 μL of Protonex™ Red 600 SE dye (AAT Bioques 21208, 10 times the molar amount of antibody), mixed and reacted at 37 °C in the dark for 1 h. Used a 50 kDa ultrafiltration tube, 4 °C, 3000×*g* centrifugation, washed with PBS to remove excess dye, stored at −80 °C for later use.

MDA-MB-468 cells were seeded at a density of 5×10^5 in confocal dishes and cultured for 24 h. Replaced with fresh medium, add fluorescently labeled antibody at a final concentration of 250 nmol/L, and incubated at 4 °C and 37 °C for 1 h, respectively. The culture was discarded, washed twice with 2 mL of pre-chilled PBS, 200 μL of PBS was added, observed and photographed using a confocal microscope, and the images were processed and analyzed using ZEN 2012 software.

*4.8. Preparation of **HN03***

Pipetted 0.5 mg of cG7-SV into a 2 mL EP tube, added 3.33 μL of TCEP (TOPSCIENCE T7087, 10 times the molar amount of antibody), pipetted and mixed well, and shook the reaction at 37 °C for 1 h. TCEP was removed by ultrafiltration at 4 °C, 3000×*g* with a 10 kDa ultrafiltration tube. Added 4 μL of DHAA (TOPSCIENCE T4917, 12 times the molar amount of antibody), mixed and shook at 27 °C for 4 h in the dark. Ultrafiltration was carried out with a 50 kDa ultrafiltration tube at 4 °C, 3000×*g* to remove DHAA. Added 3.33 μL of linker-drug **S** (10 times the molar amount of antibody), mixed and shook at 27 °C for 1 h in the dark. Ultrafiltration at 4 °C, 3000×*g* with a 50 kDa ultrafiltration tube to remove excess linker-drug **S**. The BCA kit determined the conjugate concentration and calculated the recovery, and was cryopreserved at −80 °C. **HN03-A** and **HN03-B** were prepared by the same method as above, and the conjugate small molecules were **S1** and **S2**, respectively. The preparation method of cG7-HL2 was referred to HN01[24].

*4.9. Analysis of **HN03***

The purity of the **HN03** was analyzed by SEC−HPLC (molecular exclusion chromatography) under the following detection conditions: liquid chromatograph model Agilent-1220, **HN03** concentration of 4 mg/mL, injection volume of 10 μL, mobile phase of 20 mmol/L PBS, flow rate of 1 mL/min, detector wavelength of 280 nm, column temperature of 25 °C, column model TSKgel-$G3000SW_{XL}$ (TOSOH). HIC−HPLC (hydrophobic chromatography) was used to detect the hydrophobic properties of the conjugate, and the specific experimental conditions were as follows: chromatograph model Agilent-1220, antibody concentration of 4 mg/mL, injection volume of 5 μL, flow rate of 0.4 mL/min, gradient elution, detector wavelength 280 nm, column temperature 27 °C, column model TSKgel Butyl-NPR (TOSOH). The analytical method of **HN03-A**, **HN03**-B and cG7-HL2 is the same as above.

4.10. Binding and internalization

MDA-MB-468 cells in good logarithmic condition were collected and aliquoted at 2×10^5 per tube. At 4 °C, centrifuge at 400×*g*, discard the supernatant, dilute **HN03** or cG7-SV to 100 nmol/L in L-15 complete medium, and add 250 μL per tube of cells for resuspension. Cells were placed in a 37 °C incubator, incubated for 0/10/30/60/120 min, removed and placed on ice to terminate internalization. The supernatant was discarded by centrifugation, washed twice with 500 μL of FPBS, 250 μL of FITC-goat anti-human IgG antibody (1:100, Proteintech SA00003) was added as a secondary antibody, and incubated at 4 °C for 1 h. Centrifuge discard the supernatant, wash 2 times with 500 μL of FPBS resuspend, add 350 μL of PBS to resuspend, and detect the fluorescence intensity of the FITC channel using flow cytometry. The mean fluorescence intensity (MFI) of each group of samples was plotted and analyzed using Flowjo software.

4.11. Detection of NO release

MDA-MB-468 cells with good logarithmic growth status were seeded in 24-well plates at a density of 5×10^5 and cultured until the confluence reached about 80%. Discarded the medium, washed 2 times with PBS, prepared the DAF-FM-DA probe (Beyotime S0019) working solution according to the instructions, and co-incubated with the cells at 37 °C for 20 min. On the one hand, the probes were discarded, PBS washed twice, fresh medium was replaced, **HN03** (250 nmol/L)/**CS** (1 μmol/L)/cG7-SV (250 nmol/L) was added, and the culture continued at 37 °C for 8 h. Cells were digested and collected, the supernatant was discarded by centrifugation, resuspended in PBS for 2 washes, and finally resuspended with 350 μL of PBS, and the fluorescence intensity of the FITC channel was detected by flow cytometry. Plot analysis was performed using FlowjoV10 and Prism 9.0 software. On the other hand, the probes were discarded, PBS washed twice, fresh medium was replaced, **HN03** (250 nmol/L)/**CS** (1 μmol/L)/cG7-SV (250 nmol/L)/**HN03-A** (250 nmol/L)/**HN03-B** (250 nmol/L) was added, and the culture continued at 37 °C for 5 h, washed 2 times with PBS, and observed by fluorescence microscopy.

4.12. Plasma stability

Collect human anticoagulant blood, centrifuge for 5 min at r.t, and take the upper layer of plasma for later use. The conjugate **HN03** is diluted to 10 μmol/L in plasma and incubated at 37 °C for 0 or 72 h. Plasma-incubated samples are diluted to 100 nmol/L with PBS, and changes in the binding ability of **HN03** to tumor cells are detected by flow cytometry. Plasma-incubated samples were diluted to 250 nmol/L with complete medium, and NO release of **HN03** was detected by DAF-FM-DA probe. The processing procedures for other samples are the same as those for **HN03**.

4.13. Intracellular distribution

MDA-MB-468 cells with good logarithmic growth status were seeded in confocal dishes at a density of 5×10^5 and cultured for 24 h. Replaced the fresh medium, added **HN03** at a final concentration of 250 nmol/L, incubated at 37 °C, and washed with pre-chilled PBS with shaking. Added 100 μL of fixative solution (FCMACS FMS-FP0050), incubated at r.t, and washed with PBS. Added 100 μL of permeabilization solution, incubated at r.t, and washed with 2 mL of FPBS with 5% goat serum. Added 1 mL of glycine blocking solution (0.3 mol/L, dissolved in PBS), blocked at r.t, and washed with FPBS. Added 150 μL of mouse anti-human Lamp-1 antibody (1:50, Santa Cruz Bio Sc-18821, FPBS dilution), incubated at r.t, and washed with PBS. Added a total volume of 150 μL of Alexa 488-labeled goat anti-human IgG (1:50, YERSEN 33126ES60) and Cy3-labeled goat anti-mouse IgG antibody (1:20, Proteintech SA00009-1), protected from light, incubated at r.t, and washed with PBS. DAPI staining solution (YERSEN 40728ES03) was added, incubated at r.t, and washed with PBS. Confocal microscopy was observed and images of cells under DAPI, AF488 and Cy3 channels were taken, and the images were processed using ZEN 2012 software.

4.14. Binding of *HN03* to target cells

MDA-MB-468 cells were obtained from Shanghai Cell Bank of China, CAS, Using L-15 medium (10% serum), At the time of 37 °C, culture in 100% air conditions; MDA-MB-231, CHO-S were obtained from Shanghai Cell Bank of Chinese Academy of Sciences, CHO-S-hCD24 cells for laboratory overexpressing human CD24 modified cells, using DMEM medium (10% serum). At the time of 37 °C, culture at 5% CO_2; EMT-6, SK-OV-3 cells were obtained from Shanghai Cell Bank, CAS, EMT-6-hCD24 cells were laboratory overexpressing human CD24 modified cells, using RPMI-1640 medium (10% serum). At the time of 37 °C, And were cultured in 5% CO_2. The cells with good log phase state were digested with trypsin and collected in 2×10^5 cells per tube. The cells were centrifuged at 4 °C, 400×*g* for 5 min, the supernatant was discarded, **HN03** at 100 nmol/L as primary antibody, 250 μL per tube was resuspended, and incubated on ice for 1 h. The supernatant was discarded by centrifugation, washed twice with 500 μL of FPBS, added 250 μL Alexa Fluor488-goat anti-human IgG antibody (1:200, YERSEN 33126ES60) as secondary antibody and incubated at 4 °C for 1h. The supernatant was discarded by centrifugation, washed twice in 500 μL of FPBS, resuspended with 350 μL PBS, and the fluorescence intensity of FITC channels was measured using flow cytometry. The mean fluorescence intensity (MFI) of each group was drawn and analyzed using Flowjo software.

4.15. Inhibition of cell proliferation

MDA-MB-468 cells were diluted to a density of 4×10^4 with L-15 medium with 5% serum, SK-OV-3 cells were diluted to a density of 3×10^4 with RPMI-1640 medium with 2% serum, MDA-MB-231 cells, CHO cells, and CHO-S-hCD24 cells were diluted to a density of 2×10^4 with DMEM medium with 2% serum, and EMT-6-hCD24 cells were diluted to a density of 1.5×10^4 RPMI-1640 medium with 2% serum. Each of the six cells is seeded into 96-well plates at 100 μL per well and cultured overnight. **HN03**/cG7-SV/CS wasdiluted with medium and filtered and sterilized, with a maximum dosing concentration of 1 μmol/L for **HN03** and cG7-SV and 4 μmol/L for CS, both diluted down by a 4-fold concentration gradient. Added to a 96-well plate containing tumor cells, 90 μL per well, set up a blank control (containing medium only) and a negative control (containing medium and cells) at the same time, and cultured for 72 h. Add 10 μL of MTT solution (5 mg/mL, PBS dissolve, Sangon Biotech A600799) to each well, protected from light, and continued to culture for 4 h. Took out the 96-well plate, aspirated the medium with a 1 mL syringe, added 150 μL of DMSO per well, and shook for 10 min at r.t. The absorbance at 570 nm and 630 nm was determined by microplate reader, with $OD_{570}-OD_{630}$ as the net absorption value, and the inhibition curve was plotted and the IC_{50} was calculated using Prism 9.0 software. And the inhibition rate (%) was calculated as Eq. (1):

$$\text{Inhibition rate} = (\text{Negative control} - \text{Sample}) / (\text{Negative control} - \text{Blank control}) \times 100\% \quad (1)$$

4.16. Induction of apoptosis

EMT-6-hCD24 cells with good logarithmic growth status were seeded at 6×10^4 and cultured in 6-well plates for 24 h. Discarded the medium, diluted **HN03**/cG7-SV/CS with DMEM medium with 2% serum to the indicated concentration, added to a 6-well plate, and continued to culture for 72 h. Collected the cell supernatant from the 6-well plates into a 1.5 mL EP tube,

centrifuged at 4 °C, discarded the supernatant, and collected the floating cells. Simultaneously collected the cells in the 6-well plates with EDTA-free trypsinization and mixed with the cells in the corresponding supernatant. Collected cells were centrifuged with PBS at 4 °C, 400×*g* for 3 min, and resuspended for 2 washes. Discarded PBS, resuspend with 100 μL binding buffer per tube of cells, then added 5 μL of Annexin V-FITC (YEASEN 40302ES20), mixed gently, and incubated at r.t for 15 min, keeping out of light during the whole process. 400 μL of binding buffer was added to each tube to mix, the fluorescence intensity of the FITC channel was detected by flow cytometry, and the proportion of FITC-positive cells was counted by FlowjoV10 software, and significance analysis was performed by Prism 9.0 software.

4.17. Induction of apoptosis and inhibition of metastasis pathway

EMT-6-hCD24 cells with good logarithmic growth status were seeded at a density of 1×10^5 and cultured in 6-well plates for 24 h. Discarded the medium, diluted **HN03** (250 nmol/L/500 nmol/L/1 μmol/L)/**HN03-A** (1 μmol/L)/cG7-HL2 (1 μmol/L)/cG7-SV (1 μmol/L)/**CS** (4 μmol/L) with medium containing 2% serum to the indicated concentration, added to a 6-well plate, and continued to culture for 48 h. The 6-well plate is placed on ice, washed twice with PBS per well, and then 120 μL of RIPA lysate (containing 1% cocktail and PMSF, YEASEN 20201ES60) is added. Cells were lysed, the supernatants were collected. Otherwise, RIPA lysate was added to tumor tissues (150 μL/20 mg), and then homogenized by tissue grinder at 4 °C and 60 Hz, and supernatant was collected by centrifugation (12,000×*g*). Add 5 × loading buffer (reduced) to prepare samples.

Polyacrylamide gels were prepared, with a gel concentration of 12% and a stacking gel concentration of 5%. Samples were transferred from the gel to the PVDF membrane by wet transfer at 200 mA for 90 min. The PVDF membrane was immersed in TBST containing 5% skimmed milk powder, the PVDF membrane was blocked at 37 °C for 1 h. Diluted rabbit anti p-PERK (1:1000, ABCLONAL AP1501), p-eIF2α (1:1000, ABCLONAL AP0692), DDIT3 (1:1000, ABCLONAL A21902), Bax (1:1000, ABCLONAL A19684), Caspase3 (1:1000, Proteintech 19677-1-AP), Cytochrome C (1:1000, ABCLONAL A4912), Vimentin (1:20,000, HUABIO ET1610-39) and mouse anti-human Bcl-2 (1:1000, ABCLONAL A20777), GAPDH (1:50,000, Proteintech 60004-1-Ig), β-actin (1:20,000, Proteintech 66009-1-Ig), E-Cadherin (1:1000, HUABIO EM0502) with TBST containing 2% skimmed milk powder and incubated with PVDF membrane overnight at 4 °C. PVDF membranes were washed with TBST shaking at r.t, HRP-goat anti-rabbit IgG (1:10,000, Proteintech SA00001-2) or HRP-goat anti-mouse IgG (1:40,000, Proteintech SA00001-1) were added, and incubated for 1 h at r.t. Prepared the super ECL detection reagent (YEASEN 36208ES60) according to the instructions, evenly add dropwise to the PVDF film, and immediately used the exposure instrument for detection.

4.18. Nude mouse xenograft model

Four-week-old female BALB/c nude mice were purchased from the Animal Experiment Center of Yangzhou University and kept in an SPF environment, and the environmental standards were based on the national standard of the People's Republic of China GB14925-2010. MDA-MB-468 cells with good logarithmic growth status were collected by digestion, centrifugation at 4 °C, 400×*g* for 3 min, and PBS resuspension washed 2 times. Adjusted the cell density to 1×10^7 with PBS, aspirated 100 μL of tumor cells with a syringe, punctured the needle parallel to the subcutaneous part of the nude mouse, inoculated the tumor cells into the subcutaneous part of the axillary of the right forelimb of the nude mouse, and slowly withdrew the needle to prevent cell exudation. The length (L) and width (W) of tumors and the weight of animals were measured every two days, and 8 tumors were randomly divided into groups when the tumor volume V reached 100 mm^3. The tumor volume was calculated as Eq. (2):

$$V = (L \times W^2)/2 \tag{2}$$

Experimental group: normal saline (saline) group, **HN03**-H group, **HN03**-L group, cG7-SV group, **CS** group (4 times the molar amount of antibody for administration), cisplatin group, 8 animals in each group, tail vein injection. The tumor size was measured every two days, the nude mice were euthanized after the end of administration, the tumor tissue and liver, spleen, kidney and other organs were weighed, and the tumor inhibition rate was calculated, and Prism 9.0 software was used for plotting and statistical analysis. Tumor inhibition rate was calculated as Eq. (3):

$$\text{Tumor inhibition rate}\% = (\text{Tumor weight of normal saline group} - \text{tumor weight of experimental group}) / (\text{Tumor weight of normal saline group}) \times 100\% \tag{3}$$

4.19. BALB/c mouse mammary orthotopic model

Five-week-old female BALB/c nude mice were purchased from the Animal Experiment Center of Yangzhou University and kept in an SPF environment, and the environmental standards were based on the national standard of the People's Republic of China GB14925-2010. EMT-6-hCD24 cells with good logarithmic growth status were collected by digestion, centrifugation at 4 °C, 400×*g* for 3 min, and PBS resuspension washed 2 times. The skin of the BALB/c mice were cut open to reveal the fourth pair of mammary pads. Using forceps, the mammary pad tissue was lifted and a needle was inserted to implant the tumor cells. The needle was slowly withdrawn and the area was sealed with glue to prevent cell leakage. The length (L) and width (W) of tumors and the weight of animals were measured every two days, and 8 tumors were randomly divided into groups when the tumor volume V reached 60 mm^3. The formula for calculating tumor volume was shown in Eq. (2) (see 4.18).

Experimental group 1: PBS group, **HN03**-H group, **HN03**-L group, DOX group, 6 animals in each group, peritoneal injection. The tumor size was measured every 2 days, the mice were euthanized after the end of administration, the tumor tissue and heart, lung, spleen and other organs were weighed, and the tumor inhibition rate was calculated, and Prism 9.0 software was used for plotting and statistical analysis. Tumor inhibition rate was calculated as Eq. (3) (see 4.18).

Experimental group 2: Saline group, Cisplatin group, cG7-SV + **CS** group, **HN03**-A group, cG7-HL2 group, **HN03** group, 5 animals in each group, tail vein injection. The tumor size was measured every 2 days. Blood was collected 2 days after the endpoint of dosing, and serum biochemical parameters were measured, including liver function: alanine aminotransferase

(ALT), aspartate aminotransferase (AST); renal function: creatinine (CREA), urea nitrogen (UREA); hematotoxicity: white blood cell count (WBC), platelet count (PLT). Mice were euthanized after the end of administration, the tumor tissue were weighed, and the tumor inhibition rate was calculated. The content of Pt in tumor and serum was detected by ICP−MS. Prism 9.0 software was used for plotting and statistical analysis.

4.20. Pharmacokinetic analysis in BALB/c mice

HN03 was labeled to Biotin by SiteClick Biotin Antibody Labeling Kit (Thermofisher, Cat# S20033, USA). Five BALB/c mice were injected i.v. with 10 mg/kg of **HN03**-Biotin. Blood was collected *via* tail top from mice at different points in time post-injection. The samples were left at 4 °C for 1 h. Serum was obtained by centrifuging the samples at 10,000×*g* for 5 min at 4 °C, after which serum samples were stored at −80 °C. Enzyme-linked immune sorbent assay (ELISA) was employed to detect the **HN03**-Biotin concentrations in serum. Prism 9.0 software was used for plotting and statistical analysis.

4.21. RNA sequencing

Mice were sacrificed and immersed in absolute ethanol, and tumor tissue was stripped in ultra-clean table. Tumor tissue of each group was divided into 300 mg tumor, placed in 2 mL frozen storage tubes, numbered and flash frozen in liquid nitrogen, and sent to the company for transcriptome sequencing. PCA analyze, screening of differentially expressed genes and other methods were used to analyze the sequencing results.

4.22. Immunofluorescence

The *in situ* tumors were fixed in 4% paraformaldehyde for 24 h, embedded in paraffin and made into 5 μm sections. The slices were baked in a 60 °C drying oven and placed in a tissue tank, soaked with xylene for 2 times, and then hydrated, and the samples were kept moist throughout the process. The sections are completely submerged in EDTA antigen repair solution (Beyotime P0085), heated and kept in a slightly boiling state for 15−20 min. After cooling to r.t, soak in double distilled water and PBS sequentially. Soaked the sections with 3% hydrogen peroxide solution to depleted the original peroxidase in the tissue, and then soaked them with PBS. Drew a hydrophobic closure circle around the tissue with an immunohistochemistry pen, and 0.3% PBST (Triton X-100) was added to the circle, incubated at r.t for 15 min, and was washed with TBST. Added 5% goat serum (PBS dilution) dropwise into the circle to completely cover the tissue, and blocked at r.t for 1 h. The blocking solution was discarded, and the rabbit anti-mouse CD206 antibody (1:500, 81525-1-RR) was diluted with 5% goat serum as primary antibody and incubated at 4 °C overnight. TBST (0.1% Tween 20) washed for 5 min Cy3-labeled goat anti-rabbit IgG antibody (1:50, YEASEN 33108ES60) was diluted with 5% goat serum as secondary antibody and incubated for 1 h at r.t. TBST washed for 5 min. Add a drop of DAPI Fluoromount-GTM (YEASEN 36308 ES) to the slice, cover the cover glass. The slices were scanned panoramic using NanoZoomer S60.

4.23. Statistical analysis

Analysis of normally distributed data was done using parametric tests (*i.e.*, unpaired 2-tailed student's *t*-test, one-way ANOVA) and for data not normally distributed, nonparametric tests (*i.e.*, Mann−Whitney test or Kruskal−Wallis test followed by Dunn's multiple comparisons tests). Data are presented as mean ± standard deviation (SD). All statistical analysis was done using GraphPad Prism 9 software, unless stated otherwise. *P* values less than 0.05 were considered statistically significant.

Acknowledgments

This work was supported by grants from the National Natural Science Foundation of China (82173681, 82104004, 81973223 and 82273780). This work was also supported by grants from the Natural Science Foundation of Xinjiang Uygur Autonomous Region (2022D01D38 and 2023D01D16, China), open project of the State Key Laboratory of Pathogenesis, Prevention and Treatment of High Incidence Diseases in Central Asia Fund (SKL-HIDCA-2024-4, China), Xinjiang Uygur Autonomous Region Science and Technology Support Project (2022E02123, China), Xinjiang Uygur Autonomous Region Tianshan Talent Training Program (2023TSYCCX0071, China) and the Fundamental Research Funds for the Central Universities (No. 2632023TD04, China) and "Double First-Class" University projects CPU2022PZQ15 from China Pharmaceutical University. This work was also supported by the National College Students Innovation and Entrepreneurship Training Program (202210316062Y).

Author contributions

Jianbing Wu: Methodology, Funding acquisition, Writing − original draft, Data curation, Writing − review & editing, Investigation, Conceptualization. Tianyue Cheng: Investigation, Writing − original draft, Data curation, Writing − review & editing, Methodology. Jiajun Xie: Investigation, Data curation. Ziyu Qian: Investigation, Data curation. Linhua Huang: Writing − original draft, Data curation, Methodology, Investigation. Xun Yuan: Investigation, Writing − original draft, Data curation. Libang Zhang: Investigation, Formal analysis. Shan Yang: Methodology, Project administration, Data curation. Yihua Zhang: Funding acquisition, Methodology, Project administration. Tonglin Xu: Investigation, Data curation, Project administration, Formal analysis. Juan Zhang: Funding acquisition, Investigation, Supervision, Data curation. Zhangjian Huang: Writing − review & editing, Project administration, Conceptualization, Funding acquisition, Supervision, Methodology.

Conflicts of interest

The authors declare no conflicts of interest.

Appendix A. Supporting information

Supporting information to this article can be found online at https://doi.org/10.1016/j.apsb.2025.07.037.

References

1. Foulkes WD, Smith IE, Reis-Filho JS. Triple-negative breast cancer. *N Engl J Med* 2010;**363**:1938−48.
2. Thike AA, Cheok PY, Jara-Lazaro AR, Tan B, Tan P, Tan PH. Triple-negative breast cancer: clinicopathological characteristics and relationship with basal-like breast cancer. *Mod Pathol* 2010;**23**:123−33.

3. Morante Z, Ku GADlC, Enriquez D, Saavedra A, Luján M, Luque R, et al. Post-recurrence survival in triple negative breast cancer. *J Clin Oncol* 2018;**36**:e13120.
4. Carey LA. Finding the positive in triple-negative breast cancer. *Nat Cancer* 2021;**2**:476−8.
5. Leon-Ferre RA, Goetz MP. Advances in systemic therapies for triple negative breast cancer. *BMJ* 2023;**381**:e071674.
6. Strebhardt K, Ullrich A. Paul Ehrlich's magic bullet concept: 100 years of progress. *Nat Rev Cancer* 2008;**8**:473−80.
7. Fu Z, Li S, Han S, Shi C, Zhang Y. Antibody drug conjugate: the "biological missile" for targeted cancer therapy. *Signal Transduct Targeted Ther* 2022;**7**:93.
8. Dumontet C, Reichert JM, Senter PD, Lambert JM, Beck A. Antibody−drug conjugates come of age in oncology. *Nat Rev Drug Discov* 2023;**22**:641−61.
9. Criscitiello C, Morganti S, Curigliano G. Antibody−drug conjugates in solid tumors: a look into novel targets. *J Hematol Oncol* 2021;**14**:20.
10. Beck A, Goetsch L, Dumontet C, Corvaia N. Strategies and challenges for the next generation of antibody−drug conjugates. *Nat Rev Drug Discov* 2017;**16**:315−37.
11. Arlotta KJ, Owen SC. Antibody and antibody derivatives as cancer therapeutics. *Wiley Interdiscip Rev Nanomed Nanobiotechnol* 2019;**11**: e1556.
12. Conilh L, Sadilkova L, Viricel W, Dumontet C. Payload diversification: a key step in the development of antibody−drug conjugates. *J Hematol Oncol* 2023;**16**:3.
13. Nolting B. Linker technologies for antibody−drug conjugates. *Methods Mol Biol* 2013;**1045**:71−100.
14. Walsh SJ, Bargh JD, Dannheim FM, Hanby AR, Seki H, Counsell AJ, et al. Site-selective modification strategies in antibody−drug conjugates. *Chem Soc Rev* 2021;**50**:1305−53.
15. Lhospice F, Brégeon D, Belmant C, Dennler P, Chiotellis A, Fischer E, et al. Site-specific conjugation of monomethyl auristatin E to anti-CD30 antibodies improves their pharmacokinetics and therapeutic index in rodent models. *Mol Pharm* 2015;**12**:1863−71.
16. Su Z, Xiao D, Xie F, Liu L, Wang Y, Fan S, et al. Antibody−drug conjugates: recent advances in linker chemistry. *Acta Pharm Sin B* 2021;**11**:3889−907.
17. Saber H, Simpson N, Ricks TK, Leighton JK. An FDA oncology analysis of toxicities associated with PBD-containing antibody−drug conjugates. *Regul Toxicol Pharmacol* 2019;**107**:104429.
18. Snyder SH, Bredt DS. Biological roles of nitric oxide. *Sci Am* 1992; **266**:68−71.
19. Lundberg JO, Weitzberg E. Nitric oxide signaling in health and disease. *Cell* 2022;**185**:2853−78.
20. Pervin S, Singh R, Chaudhuri G. Nitric oxide, N^{ω}-hydroxy-L-arginine and breast cancer. *Nitric Oxide* 2008;**19**:103−6.
21. Bonavida B, Garban H. Nitric oxide-mediated sensitization of resistant tumor cells to apoptosis by chemo-immunotherapeutics. *Redox Biol* 2015;**6**:486−94.
22. Oronsky B, Carter CA, Caroen S, Scribner C, Oronsky A, Reid TR. RRx-001, a first-in-class small molecule inhibitor of MYC and a downregulator of CD47, is an "erythrophagoimmunotherapeutic". *OncoImmunology* 2020;**9**:1746172.
23. Oronsky B, Guo X, Wang X, Cabrales P, Sher D, Cannizzo L, et al. Discovery of RRx-001, a Myc and CD47 downregulating small molecule with tumor targeted cytotoxicity and healthy tissue cytoprotective properties in clinical development. *J Med Chem* 2021;**64**:7261−71.
24. Sun F, Wang Y, Luo X, Ma Z, Xu Y, Zhang X, et al. Anti-CD24 antibody−nitric oxide conjugate selectively and potently suppresses hepatic carcinoma. *Cancer Res* 2019;**79**:3395−405.
25. Cheng T, Xie J, Yuan X, Guo M, Wu J, Wang M, et al. Site-specific antibody-nitric oxide conjugate HN02 possesses improved antineoplastic and safety properties. *J Immunother* 2024;**47**:149−59.
26. Fu Q, Shen S, Sun P, Gu Z, Bai Y, Wang X, et al. Bioorthogonal chemistry for prodrug activation *in vivo*. *Chem Soc Rev* 2023;**52**: 7737−72.
27. Sun T, Lv T, Wu J, Zhu M, Fei Y, Zhu J, et al. General strategy for integrated bioorthogonal prodrugs: Pt(II)-triggered depropargylation enables controllable drug activation *in vivo*. *J Med Chem* 2020;**63**: 13899−912.
28. Huang H, Dong Y, Zhang Y, Ru D, Wu Z, Zhang J, et al. GSH-sensitive Pt(IV) prodrug-loaded phase-transitional nanoparticles with a hybrid lipid-polymer shell for precise theranostics against ovarian cancer. *Theranostics* 2019;**9**:1047−65.
29. Zhang C, Zhu J, Yuan X, Yan Z, Ye H, Xiong T, et al. Development of integrated bioorthogonal self-catalyzed NO donor/platinum(IV) prodrugs for synergistical intervention against triple-negative breast cancer. *J Med Chem* 2024;**67**:479−91.
30. Wu J, Hu Y, Ye H, Zhang S, Zhu J, Ji D, et al. One stone two birds: redox-sensitive colocalized delivery of cisplatin and nitric oxide through cascade reactions. *JACS Au* 2022;**2**:2339−51.
31. Altevogt P, Sammar M, Hüser L, Kristiansen G. Novel insights into the function of CD24: a driving force in cancer. *Int J Cancer* 2021; **148**:546−59.
32. Barkal AA, Brewer RE, Markovic M, Kowarsky M, Barkal SA, Zaro BW, et al. CD24 signalling through macrophage Siglec-10 is a target for cancer immunotherapy. *Nature* 2019;**572**:392−6.
33. Barkal AA, Brewer RE, Markovic M, Kowarsky M, Barkal SA, Zaro BW, et al. CD24 signalling through macrophage Siglec-10 is a target for cancer immunotherapy. *Nature* 2019;**572**:392−6.
34. Chan SH, Tsai KW, Chiu SY, Kuo WH, Chen HY, Jiang SS, et al. Identification of the novel role of CD24 as an oncogenesis regulator and therapeutic target for triple-negative breast cancer. *Mol Cancer Therapeut* 2019;**18**:147−61.
35. Yao H, Wang Z, Wang N, Deng Z, Liu G, Zhou J, et al. Enhancing circulation and tumor accumulation of carboplatin *via* an erythrocyte-anchored prodrug strategy. *Angew Chem Int Ed Engl* 2022;**134**: e202203838.
36. Yuan S, Zhu Y, Dai Y, Wang Y, Jin D, Liu M, et al. 19F NMR allows the investigation of the fate of platinum (IV) prodrugs in physiological conditions. *Angew Chem Int Ed Engl* 2022;**61**:e202114250.
37. Zhou Q, Chen S, Xu Z, Liu G, Zhang S, Wang Z, et al. Multitargeted platinum (IV) anticancer complexes bearing pyridinyl ligands as axial leaving groups. *Angew Chem Int Ed Engl* 2023;**62**:e202302156.
38. Ferhati X, Jiménez Moreno E, Hoyt EA, Salluce G, Cabeza Cabrerizo M, Navo CD, et al. Single mutation on trastuzumab modulates the stability of antibody−drug conjugates built using acetal-based linkers and thiol-maleimide chemistry. *J Am Chem Soc* 2022;**144**:5284−94.
39. Shen BQ, Xu K, Liu L, Raab H, Bhakta S, Kenrick M, et al. Conjugation site modulates the *in vivo* stability and therapeutic activity of antibody−drug conjugates. *Nat Biotechnol* 2012;**30**:184−9.
40. Kojima H, Urano Y, Kikuchi K, Higuchi T, Hirata Y, Nagano T. Fluorescent indicators for imaging nitric oxide production. *Angew Chem Int Ed Engl* 1999;**38**:3209−12.
41. Yang C, Mu G, Zhang Y, Gao Y, Zhang W, Liu J, et al. Supramolecular nitric oxide depot for hypoxic tumor vessel normalization and radiosensitization. *Adv Mater* 2022;**34**:2202625.
42. Wang H, Guo S, Kim SJ, Shao F, Ho JWK, Wong KU, et al. Cisplatin prevents breast cancer metastasis through blocking early EMT and retards cancer growth together with paclitaxel. *Theranostics* 2021;**11**: 2442−59.
43. Shafee N, Smith CR, Wei S, Kim Y, Mills GB, Hortobagyi GN, et al. Cancer stem cells contribute to cisplatin resistance in Brca1/p53-mediated mouse mammary tumors. *Cancer Res* 2008;**68**:3243−50.
44. Ozkok A, Edelstein CL. Pathophysiology of cisplatin-induced acute kidney injury. *BioMed Res Int* 2014;**2014**:967826.
45. Gersten BK, Fitzgerald TS, Fernandez KA, Cunningham LL. Ototoxicity and platinum uptake following cyclic administration of platinum-based chemotherapeutic agents. *J Assoc Res Otolaryngol* 2020;**21**:303−21.
46. Acklin S, Zhang M, Du W, Zhao X, Plotkin M, Chang J, et al. Depletion of senescent-like neuronal cells alleviates cisplatin-induced peripheral neuropathy in mice. *Sci Rep* 2020;**10**:14170.

47. Zhu W, Shou W, Payne RM, Caldwell R, Field LJ. A mouse model for juvenile doxorubicin-induced cardiac dysfunction. *Pediatr Res* 2008; **64**:488−94.
48. Argenziano M, Gigliotti CL, Clemente N, Boggio E, Ferrara B, Trotta F, et al. Improvement in the anti-tumor efficacy of doxorubicin nanosponges in *in vitro* and in mice bearing breast tumor models. *Cancers* 2020;**12**:162.
49. Zamora P, Pozo AG, Vega Clemente L, Lopez Camacho E, Trilla Fuertes L, Alonso Martin D, et al. Abstract PO1-25-12: metformin enhances response to chemotherapy combined with immunotherapy in a triple negative breast cancer *in vivo* model. *Cancer Res* 2024;**84**: PO1-25−12.
50. Sung YC, Jin PR, Chu LA, Hsu FF, Wang MR, Chang CC, et al. Delivery of nitric oxide with a nanocarrier promotes tumour vessel normalization and potentiates anti-cancer therapies. *Nat Nanotechnol* 2019;**14**:1160−9.
51. Li F, Du X, Lan F, Li N, Zhang C, Zhu C, et al. Eosinophilic inflammation promotes CCL6-dependent metastatic tumor growth. *Sci Adv* 2021;**7**:eabb5943.
52. Cassetta L, Pollard JW. A timeline of tumour-associated macrophage biology. *Nat Rev Cancer* 2023;**23**:238−57.
53. Yang P, Yu F, Yao Z, Ding X, Xu H, Zhang J. CD24 is a novel target of chimeric antigen receptor T cells for the treatment of triple negative breast cancer. *Cancer Immunol Immunother* 2023;**72**:3191−202.
54. Guffroy M, Falahatpisheh H, Biddle K, Kreeger J, Obert L, Walters K, et al. Liver microvascular injury and thrombocytopenia of antibody−calicheamicin conjugates in cynomolgus monkeys-mechanism and monitoring. *Clin Cancer Res* 2017;**23**: 1760−70.
55. Kirchhoff D, Stelte Ludwig B, Lerchen HG, Wengner AM, Ahsen OV, Buchmann P, et al. IL3RA-targeting antibody−drug conjugate BAY-943 with a kinesin spindle protein inhibitor payload shows efficacy in preclinical models of hematologic Malignancies. *Cancers (Basel)* 2020;**12**:3464.
56. Shi M, Zhang J, Wang Y, Peng C, Hu H, Qiao M, et al. Tumor-specific nitric oxide generator to amplify peroxynitrite based on highly penetrable nanoparticles for metastasis inhibition and enhanced cancer therapy. *Biomaterials* 2022;**283**:121448.
57. Deng X, Apple S, Zhao H, Song J, Lee M, Luo W, et al. CD24 Expression and differential resistance to chemotherapy in triple-negative breast cancer. *Oncotarget* 2017;**8**:38294−308.
58. Panowski S, Bhakta S, Raab H, Polakis P, Junutula JR. Site-specific antibody drug conjugates for cancer therapy. *mAbs* 2014;**6**: 34−45.
59. Sanomachi T, Okuma HS, Kitadai R, Kawachi A, Yazaki S, Tokura M, et al. Low HER2 expression is a predictor of poor prognosis in stage I triple-negative breast cancer. *Front Oncol* 2023; **13**:1157789.